E G B

NEUTRON RESONANCES IN THE NICKEL ISOTOPES AND OTHER INTERMEDIATE NUCLEI

by

John Alden Farrell

Department of Physics
Duke University

Date: April 22 1964

Approved:

Henry W. Newson
Henry W. Newson, Supervisor

E. G. Bilpuch
Eugene Greuling
Horst Kaper
J. M. Gallie Jr.

A dissertation submitted in partial fulfillment of the requirements for the degree of Doctor of Philosophy in the Department of Physics in the Graduate School of Arts and Sciences of Duke University

1964

ABSTRACT

(Physics)

NEUTRON RESONANCES IN THE NICKEL ISOTOPES AND OTHER INTERMEDIATE NUCLEI

by

John Alden Farrell

Department of Physics
Duke University

Date: _____

Approved:

_____
Henry W. Newson, Supervisor

_____

_____

_____
Horst Heyer

_____
J. M. Galli, Jr.

An abstract of a dissertation submitted in partial fulfillment of the requirements for the degree of Doctor of Philosophy in the Department of Physics in the Graduate School of Arts and Sciences of Duke University

1964

ABSTRACT

NEUTRON RESONANCES IN THE NICKEL ISOTOPES AND OTHER INTERMEDIATE NUCLEI

by

John Alden Farrell

High resolution neutron total cross sections of separated isotopes of Ca^{42}, Ca^{44}, Cr^{50}, Cr^{54}, Ni^{58}, Ni^{60}, Ni^{62} and Ni^{64} have been measured using the Li^7 (p,n)Be^7 reaction as the source of neutrons. The data have been fitted with a multilevel formula derived from the R matrix formalism. Widths have been obtained for all recognizable s wave resonances and a few of the widest p wave resonances. The distributions of the reduced widths and local spacings of the s wave resonances were found to be in good agreement with the respective Porter-Thomas and Wigner distributions. The average s wave level spacings have been corrected to an excitation energy of 6 mev and combined with data for other nuclei in this region in order to compare the behavior of the average level spacings with the predictions of various shell models. We obtain reasonably good agreement with both the Rosenzweig model and the model of Newson and Duncan if we assume that, at the excitation energies involved, a major shell is closed at 16 nucleons instead of 20. The data indicates that a dependence of the average level spacing on neutron excess exists but that it probably is not a simple exponential.

ACKNOWLEDGEMENTS

I wish to express my deep appreciation to my research advisor, Professor H.W. Newson, whose suggestions and support made these experiments possible. Professor E.G. Bilpuch worked closely with me during all phases of this research and rendered invaluable aid. I wish to thank all members of the Duke University Nuclear Structure Laboratory, particularly Messrs. P.M. Beard, M. Divadeenam, G.C. Kyker, Jr., P.B. Parks and R.H. Tabeney for their assistance in taking the data. In addition, Mr. G.C. Kyker, Jr. furnished several computer programs which were of particular value in analysing the data. Messrs. S.E. Edwards and O.C. Duncan were of great help in keeping the electronic equipment in working order. I am also indebted to the members of the Instrument Shop, particularly Messrs. M. Whitfield and A. Lovette for their aid in the construction of portions of this apparatus. I owe special thanks to Mrs. Dorothy Lore for her aid in the data reduction and to Mr. William Meier and Mrs. J.N. Bailey for their excellent draftsmanship. Analysis of the data would have been impossible without the wholehearted cooperation of the Duke University Digital Computing Laboratory. I owe my greatest debt of gratitude to my wife, Lou Ann, and to my Mother for their encouragement during these years of study. This work was supported in part by the United States Atomic Energy Commission.

J. A. F.

CONTENTS

LIST OF FIGURES

LIST OF TABLES

NEUTRON RESONANCES IN THE NICKEL ISOTOPES AND OTHER INTERMEDIATE NUCLEI

CHAPTER I

INTRODUCTION

During the last ten years, the Duke University Nuclear Structure Laboratory has been carrying out a systematic study of neutron resonances in the kev region. The Ph.D. theses of Rohrer (1954); Gibbons (1954); Marshak (1956); Block (1956); Patterson (1955); Toller (1954); and Bowman (1961) are based on this work as well as the M.A. theses of Smith (1955); Crutchfield (1955); Bowman (1958); Karriker (1956); and Chern (1954). The later results have been published in a series of papers in the Annals of Physics entitled "s- and p- Wave Neutron Spectroscopy". Eight parts of this series have been published and four more are in the process of preparation. Part XII will be based in part on the work reported in this thesis. We shall refer to these papers as Parts I, II, etc. in the following discussion.

In the early work of Patterson (1955), it was noticed that in the total cross section curves of the two isotopes of chlorine, Cl^{35} and Cl^{37}, the most prominent resonances at low energy occur at 25 $\pm$ 0.5 kev in each compound nucleus. There are also (see Part X) a half dozen other resonances in each cross section curve which correspond rather closely in energy to peaks in the other. This surprising observation prompted measurements on a number of pairs of isotopes which differed two or four units, and other cases of coincidence of energy were observed. However, while it seemed unlikely that these were chance coincidences, their occurrence was not consistent enough to allow any definite

interpretation. The most striking of these coincidences were observed in the cross section curves of Ni^{58} and Ni^{60} where 80% of the observed resonances below 200 kev showed this isotopic coincidence (Newson et al., 1959). A crucial experiment has long been planned: the measurement of all stable even-even isotopes of nickel to see if three or four fold coincidences among the resonances of isotopes could be observed with anything like the frequency of the two fold coincidences between Ni^{58} and Ni^{60}. Unfortunately, Ni^{62} and Ni^{64} are not very abundant but reasonably pure samples of these two isotopes became available recently. Even so, the size of the samples was quite small and new methods of measurement had to be developed in order to measure their cross section curves. At the same time, small but again quite pure samples of Ca^{42}, Ca^{44}, Cr^{50} and Cr^{54} were measured with some of the same difficulties. Combining these data with earlier measurements by Bowman, Bilpuch and Newson, (1962), we can also look for triple coincidence among the isotopes of calcium, chromium and titanium although the sample purities of the latter were not very satisfactory.

A search for multiple coincidences in the resonances of all these isotopes revealed very little. More triple coincidences were observed in nickel than in any of the other elements but there were no quadruples at all. Furthermore, when the E_0 values obtained from R matrix analysis were compared, the coincidences became less striking than when the observed maxima of the cross sections near the resonance energy were considered. Thus, while we feel that there is probably something interesting to be found out about relative resonance energies in isotopes differing by two mass units, we have at present no interesting conclusions to report. We will continue to seek a solution of this riddle.

In spite of disappointing results on the resonances of isotopes, this work produced new and accurate cross section curves of Ca^{42}, Ni^{62} and Ni^{64}. In addition, we have extended and greatly improved our older measurements on Ca^{44}, Cr^{50}, Cr^{54}, Ni^{58} and Ni^{60}. In general, the older work done with the 122° collimator was quite adequate for resonances below 50 kev and comparable in some cases with our newer results up to nearly 100 kev. However, the number of accurately fitted and well known resonances above 100 kev has been greatly increased by this work. In the final section we will interpret the new results together with those of Bowman in terms of the Rosenzweig, (1957) model and the Newson and Duncan, (1959) supershell model. The agreement with the models in the tentative form proposed is very gratifying. We believe that these experimental results warrant further theoretical studies of supershell models.

CHAPTER II

EXPERIMENTAL CONDITIONS

Neutron Energy Spread

The experimental arrangement was much the same as that described in Parts IV and VIII except that the apparatus was moved to the Duke 3 mev electrostatic accelerator which afforded better stability and less proton energy spread. The two port system and the homogenizer were used (Parks, Newson and Williamson, 1958).

The source of neutrons was a thin lithium target evaporated in the target chamber as described in Part VIII. The effective neutron energy spread could be determined by observing the minimum observed widths of the narrow p-wave resonances that were present in all of the samples. In general, the resolution agreed with that shown in Part VIII when the targets were fresh, but the targets gradually deteriorated with use so that in practice, we were unable to maintain this optimum resolution. However, in the 20° measurements, the energy spread was always less than 1.5 kev above a neutron energy of 150 kev.

Background

Background in this experiment can arise from three sources: normal counter background, background from neutrons penetrating the shielding of the

collimator and neutrons emitted at some angle other than 20° which are scattered into the collimator either by the sample or by the target backing. The first two are easily measured and were found to be less than the counting statistics(approximately 1% of the total count). The other background was estimated by observing the depression in peak height of a fully resolved resonance. The background was found to be so small as to be difficult to measure and amounted to 5% or less of the total count. With the sample thicknesses used, background introduced an error of less than 0.5 barn over most of the energy range observed. Because of the small amount of background present and the uncertainty in its measurement, no background correction was deemed necessary.

Transmission Measurement

Transmission ratios were measured for the separated isotopes: Ca^{42}, Ca^{44}, Cr^{50}, Cr^{54}, Ni^{58}, Ni^{60}, Ni^{62} and Ni^{64}. Table I gives sample thicknesses, contaminants, total counts, and energy range measured for each sample. Most of the samples were furnished as 15 to 20 grams of powder. These were pressed in a die with 1 inch by $\frac{1}{2}$ inch face dimensions and canned in 2 mil silver foil. Transmission measurements on these samples were made with the 20° collimator as described in Part VIII.

Two of the samples (Cr^{54} and Ni^{64}) were furnished in the form of small disks approximately 1 centimeter in diameter and weighing 3 to 5 grams. These samples were too small to position over one counter bank at a time and a new sample changer was made for them. It positioned the sample over both banks in one position and completely removed it in the other. Because of the

Table I. Sample Thicknesses

Nucleus	Energy Range Kev	N Element 10^{22} atoms/cm^2	N Oxygen 10^{22} atoms/cm^2	Open Beam Counts
Ca^{42}	30 - 650	3.19	3.46	10,000
Ca^{44}	30 - 650	3.32	3.48	"
Cr^{50}	40 - 620	3.16	5.24	"
Cr^{54}	100 - 595	2.64	1.82[a]	"
Ni^{58}	90 - 654	6.49	0.00[b]	"
Ni^{60}	30 - 652	6.29	0.00	"
Ni^{62}	3 - 656	6.10	0.00	10,000[c]
Ni^{64}	30 - 650	3.80	0.00	"

a. Two samples were used together, one Cr metal, N = 1.42×10^{22} atoms/cm^2, the other Cr_2O_3, N chromium = 1.22×10^{22}, N oxygen = 1.82×10^{22} atoms/cm^2.

b. The presence of a small oxygen contamination is indicated by a slightly high cross section in the region of the oxygen resonance at 435 kev.

c. A total open beam count of 4,000 was taken in the 160° measurements.

use of the homogenizer, it was necessary to construct a special transistorized current integrator to control the counting time. The integrator was placed between the homogenizer and the target chamber and consequently operated at homogenizer potential. Control of the integrator was accomplished by the use of lights and photocells.

In order to observe the low energy resonances of Ni^{62}, the neutron collimator was rotated on its gun mount to the 160° position. In this position, it was necessary to place the sample inside the vacuum chamber. The sample shadowed only one bank and was not moved during the experiment. The unshadowed bank was used as a monitor. This method is unsuited for the measurement of absolute cross sections because no compensation can be made for variations of efficiency of one bank relative to the other, but the observation of the resonance structure is feasible.

Analysis

The output from the recording scalers was punched onto cards and reduced to cross sections using the Duke I.B.M. 7072 computer.

The level spacing of the compound nuclei is small enough that resonance-resonance interference makes area analysis impractical. Therefore, a shape fit to the cross sections has been made using a multilevel formula derived from R Matrix theory as described in Part VIII, but a new computer program has been written that includes the effects of experimental resolution. This has made possible a better fit near the narrower resonances. The fit is made by trial and error by superimposing a computer plot of a calculated cross section over a similar plot of the experimental data.

All recognizable s wave resonances and the wider p wave resonances have been fitted by this procedure. Very few of the p wave resonances were resolved sufficiently well to permit a determination of their spins. Some of the smaller p wave resonances were included in the multilevel formula to improve the appearance of the fit but accurate parameters could not be determined for them. Due to the nature of the computer program, it was not possible to include p wave resonances with a true width less than the spacing between points.

The calcium and chromium samples were furnished as oxides. The oxygen cross section was obtained by measuring and subtracting the total cross section of Be from that of BeO. The resulting oxygen data was plotted and a smooth curve drawn through the points. Values of the oxygen cross section were then read from the curve and punched onto cards for use in correcting the other data.

Subtraction of the oxygen increased the point scatter of the data somewhat. This scatter was considerably reduced by making a three point running average of the data for all samples containing oxygen. No smoothing was necessary for the nickel isotopes which were metallic.

The Cr^{54} sample apparently contained a small amount of water as its cross section was high at the lower energies, even in the interference minima of wide s wave resonances. Accordingly, enough water cross section was subtracted to bring the interference minima to zero.

The fits were improved at the ends of the energy regions measured by including fictitious resonances outside the range as described in Part VIII and also by not attempting to fit the upper 50 kev of the data. Unambiguous fits of some of the data became difficult at energies greater than 300 to 400

kev because of the appearance of many poorly resolved p or d wave resonances that tended to obscure the s wave structure.

The resonance energies quoted are $(E_\lambda + \Delta_\lambda)$, where E_λ is the R Matrix energy and Δ_λ is the single level shift factor. For relatively isolated resonances, these energies are the same as would be used in the single level Breit-Wigner formula.

CHAPTER III

EXPERIMENTAL RESULTS

S wave level parameters obtained from the multilevel fits are listed in Table II. Resonance energies and widths, where available, are shown in Table III for all apparently statistically significant non s wave peaks.

Calcium

The calcium samples were furnished as powdered oxides. The data was corrected for oxygen and then smoothed by making a three point running average to reduce the point scatter. Some difficulty was encountered in fitting the data in the neighborhood of the oxygen resonance where a small uncertainty in the position (E_o) of the oxygen resonance can cause considerable error. By making small adjustments in its position for each sample, fairly satisfactory fits of this region were obtained but the results are not as good as in the surrounding regions.

Ca^{42}. The experimental data for the calcium isotopes are shown in Figures I, II and III. The solid curve is the multilevel fit to the data. No fit was attempted below 100 kev where two groups of neutrons were present or above 600 kev where the effects of resonances above 650 kev were unkown and could not be taken into account. A peak was observed at 40 kev that was

Table II. S Wave Resonance Parameters

Isotope	E_o (kev)	Γ (kev)	Γ_n^o (ev)
Ca^{42}	40.0[a]	5.0	25.0
	124.2	3.75	10.641
"	128.5	11.00	30.686
"	157.7	0.30	0.755
"	175.0	2.50	5.976
"	213.2	1.75	3.790
"	259.5	0.75	1.472
"	274.5	0.75	1.431
"	278.5	1.50	2.842
"	356.5	1.50	2.512
"	399.5	0.50	0.791
"	418.0	0.40	0.619
	425.0	0.30	0.460
	450.5	1.75	2.607
"	468.5	0.30	0.438
"	478.0	0.75	1.085
"	491.5	1.00	1.426
"	513.5	5.50	7.675
"	532.0	6.50	8.912
"	545.5	2.00	2.708
"	555.0	0.30	0.403
"	560.0	0.50	0.668
"	570.5	10.00	13.240

Table II (continued)

Isotope	E_o (kev)	Γ (kev)	Γ_n^o (ev)
Ca^{44}	22.0[b]	0.54	3.6
"	53.0[a]	3.0	13.0
"	103.0	5.50	17.137
"	147.3	10.00	26.055
"	158.5	0.30	0.754
"	175.0	1.50	3.586
"	247.0	3.00	6.036
"	321.5	9.00	15.873
"	370.0	11.00	18.084
"	385.0	0.30	0.483
"	402.0	2.75	4.337
"	443.5	1.50	2.252
"	483.0	17.50	25.181
"	506.0	3.50	4.920
"	530.0	2.00	2.747
"	538.5	0.50	0.681
"	546.0	0.80	1.083
	560.5	2.50	3.339

Table II (continued)

Isotope	E_o (kev)	Γ (kev)	Γ_n° (ev)
Cr^{50}	6.6[b]	1.7	21.0
	28.7[b]	0.51	3.0
"	38.7[b]	1.82	9.4
"	43.9[b]	0.65	3.1
"	95.5	2.25	7.355
"	130.0	0.75	2.109
"	157.5	1.75	4.484
"	163.3	0.80	2.014
"	186.5	3.00	7.085
"	232.5	1.50	3.188
	258.0	0.50	1.011
"	278.0	2.50	4.882
"	292.0	6.00	11.449
"	307.0	1.50	2.796
"	322.0	7.00	12.759
"	327.7	0.50	0.904
"	353.0	5.50	9.605
"	359.5	1.75	3.030
"	370.0	10.00	17.087

Table II (continued)

Isotope	E_o (kev)	Γ (kev)	Γ_n^o (ev)
Cr^{50}	388.5	4.00	6.683
"	395.0	0.25	0.415
"	413.7	1.75	2.841
"	416.5	14.00	22.655
"	433.5	10.00	15.889
"	454.5	0.25	0.389
"	467.5	6.50	9.980
"	478.0	2.50	3.800
"	489.0	1.75	2.633
"	502.5	4.00	5.945
"	515.0	2.00	2.940
"	523.0	0.50	0.730
"	538.5	3.00	4.323
"	547.0	2.50	3.577
"	553.8	6.00	8.538
"	560.5	3.00	4.246
"	578.0	2.70	3.770
"	580.5	7.00	9.755
"	590.7	1.50	2.074

Table II (continued)

Isotope	E_o (kev)	Γ (kev)	Γ_n^o (ev)
Cr^{54}	23.5[b]	0.49	3.2
"	26.5[b]	0.50	3.1
"	118.5	4.50	13.072
"	174.5	1.70	4.070
"	283.0	8.50	15.978
"	329.0	8.50	14.819
"	337.5	0.25	0.430
"	344.0	0.30	0.511
"	351.5	0.35	0.590
"	432.5[a]	5.0	5.0
"	451.0[a]	2.0	3.0
"	486.5[a]	8.0	11.5
Ni^{58}	16.5[b]	1.54	11.989
"	60.0[b]	3.56	14.534
"	107.0	2.00	6.114
"	122.5	1.00	2.857
"	136.0	3.00	8.135
"	138.5	3.00	8.061
"	157.0	6.25	15.774
"	167.5	0.50	1.222

Table II (continued)

Isotope	E_o (kev)	Γ (kev)	Γ_n° (ev)
Ni^{58}	190.5	3.00	6.873
	204.5	7.50	16.585
	231.0	6.00	12.484
	243.0	0.25	0.507
"	270.0	6.00	11.547
"	278.0	2.00	3.793
"	303.5	0.75	1.361
"	325.0	2.00	3.508
"	349.0	1.50	2.539
"	367.0	0.25	0.413
"	394.0	0.75	1.195
"	417.5	5.00	7.738
"	426.5	8.00	12.250
"	454.5	3.00	4.450
"	461.5	0.75	1.104
"	495.5	2.00	2.841
"	507.0	2.00	2.809
"	522.5	0.75	1.038
"	571.0	10.00	13.234
"	588.5	2.50	3.259
	600.0	6.00	7.746

Table II (continued)

Isotope	E_o (kev)	Γ (kev)	Γ_n^o (ev)
Ni^{60}	14.5[b]	2.60	21.640
"	30.0[b]	1.10	6.380
"	62.0[b]	0.70	2.838
"	84.5[b]	0.50	1.742
"	96.5	1.25	4.084
"	106.0	0.84	2.622
"	160.0	1.80	4.611
"	186.2	6.00	14.303
"	197.0	3.50	8.125
"	257.0	3.75	7.690
"	316.0	3.20	5.969
"	325.0	8.50	15.655
"	338.0	5.25	9.500
"	346.0	0.25	0.443
"	357.2	1.00	1.765
"	375.5	4.00	6.905
"	412.3	0.75	1.242

Table II (continued)

Isotope	E_o (kev)	Γ (kev)	Γ_n^o (ev)
Ni^{60}	421.0	2.00	3.282
"	426.5	0.50	0.816
"	436.0	1.00	1.616
"	446.0	3.00	4.800
"	453.0	1.50	2.384
"	462.0	1.00	1.576
"	473.0	0.50	0.780
"	484.6	3.75	5.788
"	498.0	5.00	7.628
"	513.5	2.25	3.388
"	520.3	5.00	7.486
	525.5	3.00	4.473
"	533.0	0.50	0.741
"	556.5	0.50	0.728
"	580.3	0.25	0.357
"	588.5	0.50	0.711
"	594.8	2.50	3.538

Table II (continued)

Isotope	E_o (kev)	Γ (kev)	Γ_n^o (ev)
Ni^{62}	6.0[a]	10.0	130.0
	42.5[a]	1.0	4.9
"	56.5[a]	0.2	0.83
"	93.5	2.25	7.483
"	104.5	4.50	14.183
"	148.5	0.20	0.533
"	229.5	7.25	15.761
"	242.2	0.75	1.591
"	280.5	5.50	10.911
"	286.0	1.50	2.950
	304.0	0.80	1.531
"	327.0	5.50	10.186
"	344.2	7.50	13.578
"	356.2	2.00	3.567
"	374.5	0.25	0.436
"	382.5	1.25	2.161
"	388.5	4.50	7.726
"	401.2	1.90	2.540

Table II (continued)

Isotope	E_o (kev)	Γ (kev)	Γ_n^o (ev)
Bi^{62}	423.0	1.50	2.483
"	433.0	6.50	10.650
"	444.0	0.35	0.567
"	456.0	0.50	0.800
"	475.0	1.50	2.363
"	488.5	4.00	6.228
"	498.0	1.50	2.317
"	508.5	0.50	0.766
"	539.0	2.00	2.989
"	571.8	4.00	5.836
"	581.0	0.50	0.725
"	583.5	10.00	14.471
"	590.5	2.00	2.880
Bi^{64}	33.0[a]		
"	128.8	1.70	4.847
"	154.5	5.00	13.076
"	163.0	0.30	0.765
"	177.5	0.50	1.225
"	231.0	4.00	8.670

Table II (continued)

Isotope	E_o (kev)	Γ (kev)	Γ_n^o (ev)
Ni^{64}	268.0	3.00	6.076
"	298.0	1.00	1.930
"	306.5	1.50	2.851
"	333.0	0.25	0.459
"	340.2	0.50	0.910
"	389.0	6.00	10.296
"	420.8	8.00	13.270
"	483.0	5.00	7.822
"	523.0	1.00	1.513
"	529.3	0.75	1.129
"	536.5	10.00	14.976
"	552.0	2.00	2.960
"	576.0	4.00	5.819
	583.0	0.30	0.434

a. Observed in cross section but outside of the region fitted, widths are estimated.

b. Data from Part VII.

Table III Non S Wave Resonance Parameters

Isotope	E_o (kev)	Γ (kev)	g
Ca^{42}	189.0		
"	221.5		
"	238.5	0.5	2
"	249.0		
"	254.0	0.8	1
"	275.0		
	280.5	0.75	1
"	297.0		
"	334.0		
	338.0		
	378.5		
	385.0		
"	445.0		
"	447.0	1.0	2
"	497.5		
"	509.0		
"	564.5		
	572.5		

Table III (continued)

Isotope	E_o (kev)	Γ (kev)	ε
Ca^{44}	133.0		
"	137.5		
"	160.0		
"	213.5		
"	221.0	0.8	1
"	272.5		
"	288.5		
"	306.5		
"	309.0		
"	316.0		
"	332.5		
"	361.5		
"	379.5		
"	438.3	2.0	1
"	448.5		
"	454.0		
"	461.0		
"	472.0		
"	475.5	2.0	1
"	490.0	1.0	1

Table III (continued)

Isotope	E_o (kev)	Γ (kev)	S
Ca^{44}	495.0		
"	503.0		
"	525.5		
"	557.0		
"	568.0		
"	576.0	0.75	1
Cr^{50}	113.0		
"	116.5		
"	122.0		
"	142.0		
"	283.5		
	313.5	0.65	2
"	341.0		
"	348.0		
"	381.0		
"	405.0	0.5	2
"	431.5	0.5	2
"	442.0		
"	459.5	0.75	1
"	472.0	0.75	1
"	509.0		
"	536.0		

Table III (continued)

Isotope	E_o (kev)	Γ (kev)	ε
Cr^{54}	189.0		
"	248.0		
"	357.5		
"	363.5		
"	377.5		
	386.5	0.6	2
	440.5		
"	470.0		
"	504.0		
"	530.0		
"	560.0		
Ni^{58}	147.5		
"	183.5		
"	215.0		
"	247.5		
"	257.5		
"	286.5		
"	306.5		

Table III (continued)

Isotope	E_o (kev)	Γ (kev)	ε
Ni^{58}	334.5		
"	343.5		
"	357.5		
"	378.5		
"	396.5		
"	413.0		
"	416.0		
"	426.0	0.5	2
"	435.5		
"	446.0		
"	451.0		
"	458.5		
"	492.5		
"	508.0		
"	512.5		
"	530.0		
"	544.0		
"	554.5	1.25	1
"	559.5		

Table III (continued)

Isotope	E_o (kev)	Γ (kev)	ε
Ni^{60}	126.5		
"	138.5		
"	156.0		
"	206.0		
"	214.0		
"	220.0		
"	229.0		
"	252.0		
"	282.5		
"	292.5		
"	306.0		
"	358.5		
"	378.5		
"	387.5		
"	392.0		
"	397.0		
"	401.5		
"	431.5		
"	497.5		
"	502.5		
"	511.5	1.0	2
"	552.5		
"	566.0		

Table III (continued)

Isotope	E_0 (kev)	Γ (kev)	g
Ni^{62}	137.5		
"	189.5		
"	216.5		
"	259.5		
"	272.5		
"	297.0		
"	299.5		
"	315.5		
"	319.0		
"	323.0		
"	352.0		
	364.0		
"	403.3		
"	420.3		
"	446.5		
"	449.8		
"	450.0		
"	461.8		
"	480.0		
"	493.5	1.0	1

Table III (continued)

Isotope	E_o (kev)	Γ (kev)	g
Ni^{62}	515.5		
"	522.0		
"	529.0	0.75	2
"	535.5	0.9	1
"	554.0		
"	568.5		
"	599.5	1.0	1
Ni^{64}	105.0		
"	141.5		
"	191.0		
"	213.7		
"	235.7		
"	254.0		
"	274.0		
"	289.0		
"	320.0		
"	326.5		
"	334.0		
"	352.0		
"	360.3		

Table III (continued)

Isotope	E_0 (kev)	Γ (kev)	ℓ
Ni^{64}	365.0	0.9	2
"	368.0		
"	371.5	0.6	2
"	376.0		
	383.0	0.65	2
"	392.5		
"	395.5		
"	407.0	1.0	2
"	414.0		
"	455.5	0.75	1
"	459.5	0.5	2
	466.5	1.0	1
	470.0		
	479.0	1.0	1
	487.8		
"	499.5		
"	503.0		
"	519.0		
"	541.5	0.8	2
"	565.0		

Figure 1. Calcium ^{42} and Calcium ^{44} 30-240 kev.

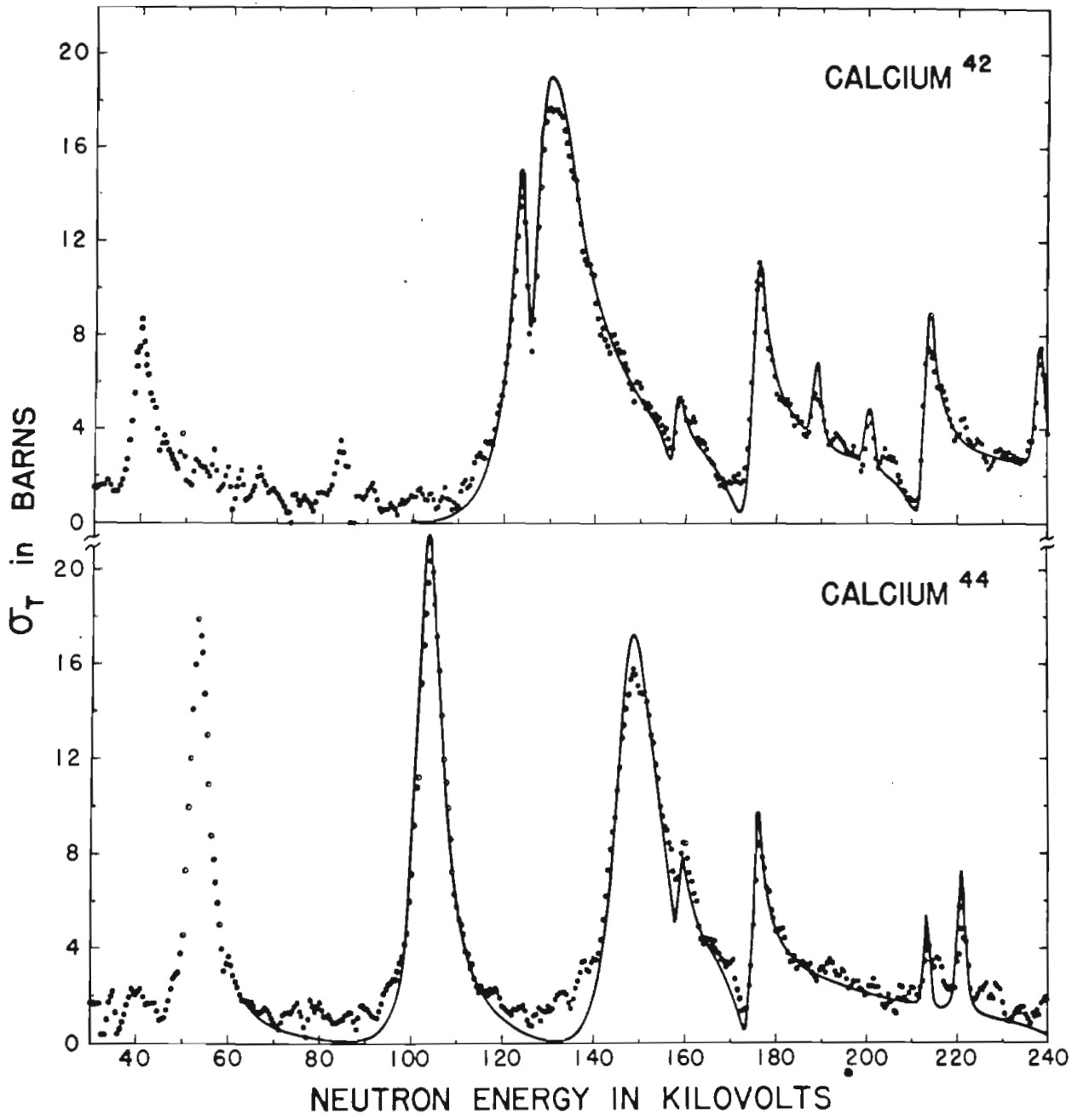
CALCIUM 42
CALCIUM 44
σ_T in BARNS
NEUTRON ENERGY IN KILOVOLTS
0
4
8
12
16
20
40
60
80
100
120
140
160
180
200
220
240

Figure 2. Calcium ^{42} and Calcium ^{44} 240-450 kev.

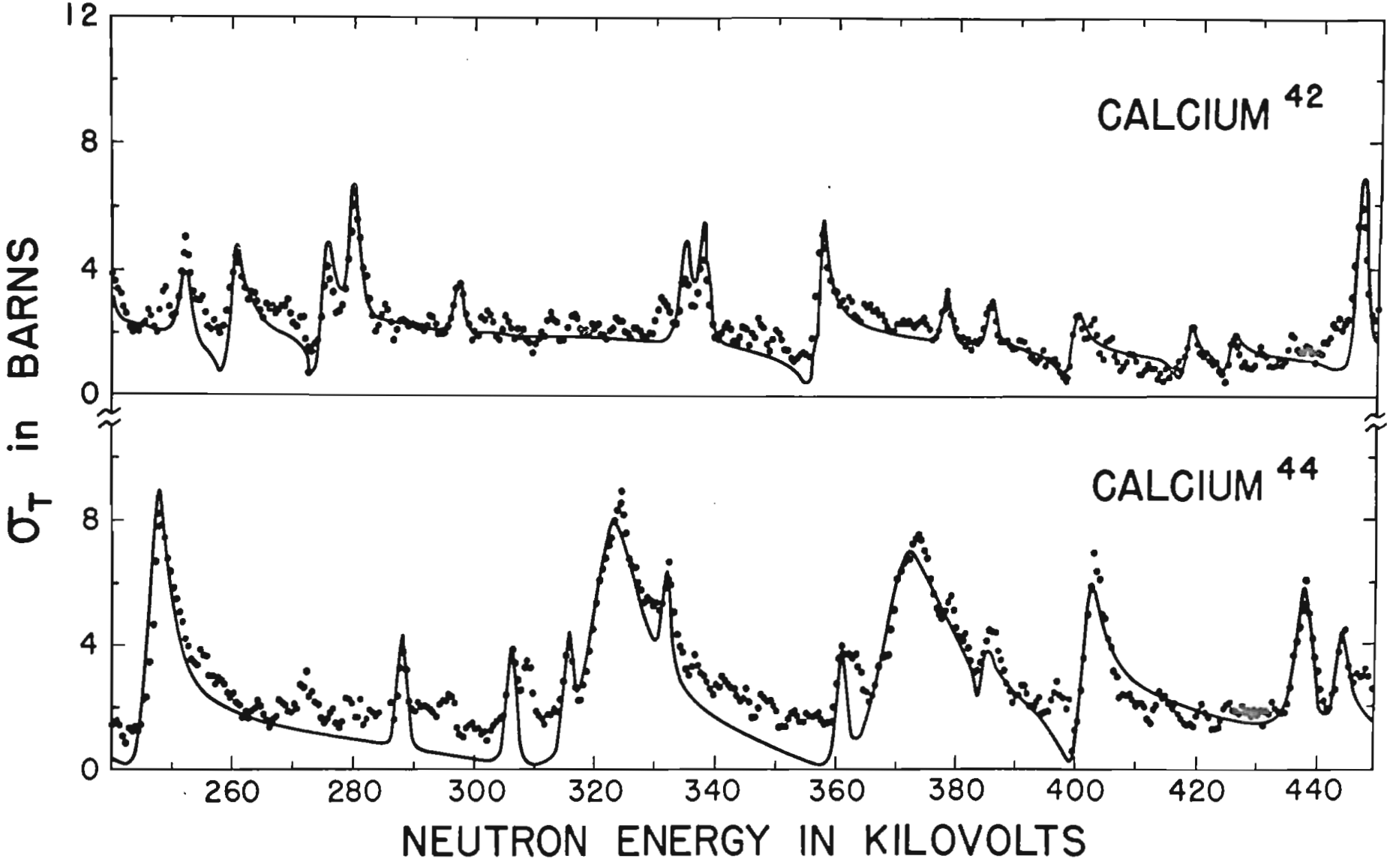
CALCIUM 42
CALCIUM 44
σ_T in BARNS
0
4
8
12
260
280
300
320
340
360
380
400
420
440
NEUTRON ENERGY IN KILOVOLTS

Figure 3. Calcium^{42} and Calcium^{44} 450-650 kev.

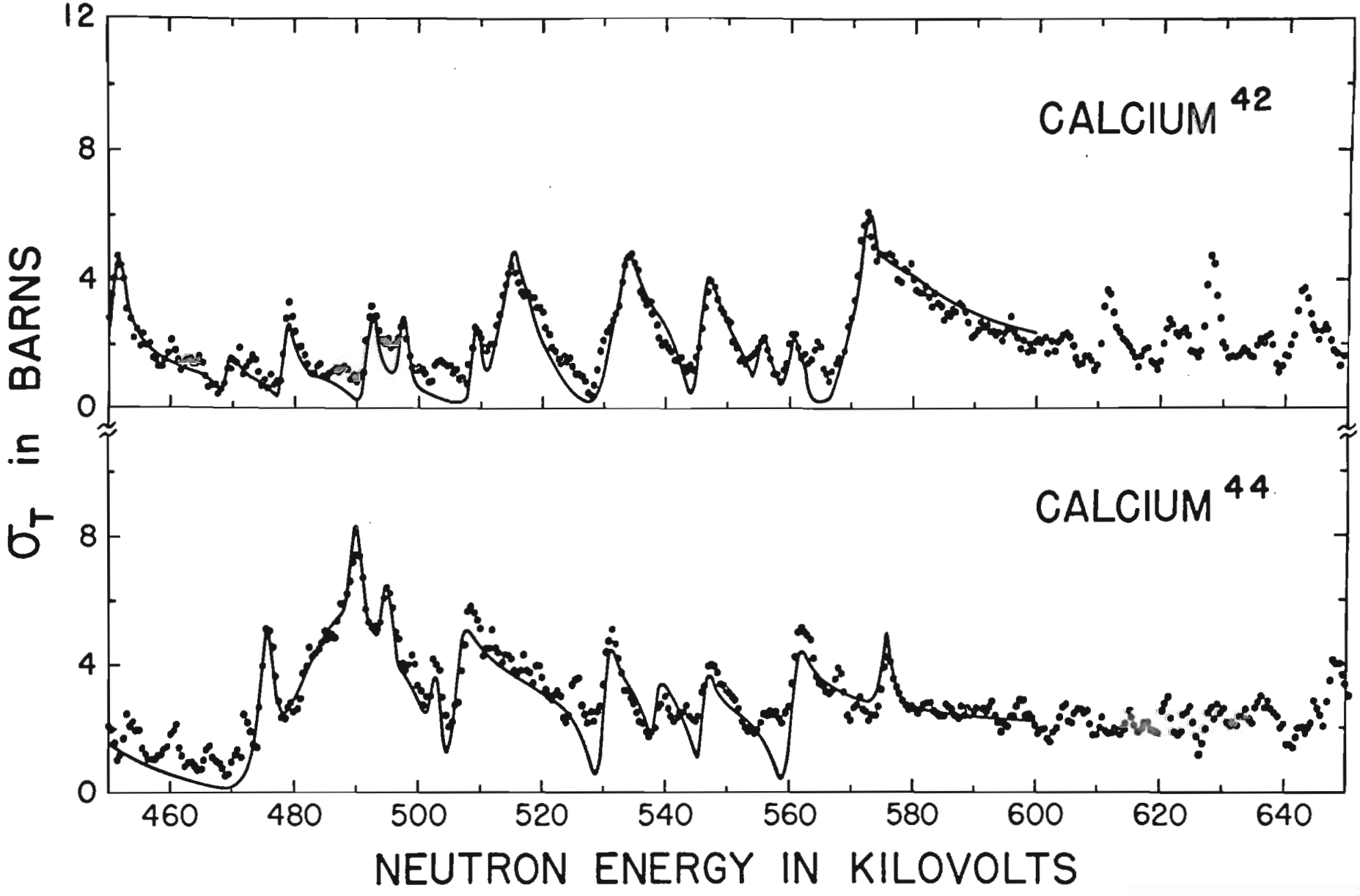
CALCIUM 42
CALCIUM 44
σT in BARNS
NEUTRON ENERGY IN KILOVOLTS
0
4
8
12
460
480
500
520
540
560
580
600
620
640

not fitted because of the large neutron energy spread and the two groups of neutrons present. The energy of this resonance was taken to be 40 kev rather than the second group energy of 15 kev because if the peak had been observed in the second group, the position of the interference minimum would be reversed.

The s wave resonances are readily distinguished by the interference minima on the low energy sides of the resonances and by their asymmetric shape. For example, the resonances at 175 and 213 kev clearly exhibit the typical s wave shape whereas the resonance at 238 kev has no minimum or high energy tail and therefore has been interpreted as a p wave.

The structure at 130 kev is composed of two strongly interfering s wave resonances, one 3.75 kev wide at 124.2 kev, the other 11 kev wide at 128.5 kev.

The resonance at 447 kev must be interpreted as an $\ell = 1$, $J = 3/2$ resonance since it is located in the interference minimum of the s wave resonance at 450.0 kev and rises well above $4\pi\lambda^2$. This is one of the few instances in which it has been possible to determine the spin of a p wave resonance in this data.

There are many other small non s wave resonances throughout the data that have the effect of obscuring the s wave structure and making an exact fit of the data difficult. No attempt was made to include all of these small resonances although the largest ones have been included in the multilevel formula to improve the visual appearance of the fit.

Above 500 kev the cross section increases in complexity with several s wave resonances that are strongly distorted by resonance-resonance interference.

The resolution function used for this fit was 2.0 kev below 150 kev and 1.5 kev above.

Ca^{44}. This cross section curve is difficult to fit unambiguously because of its low potential phase shift (kR'), the presence of a number of large s wave resonances which reduce the potential scattering even further on their low energy sides, and many non s wave resonances, some of which are relatively wide. Many of the smaller s wave resonances are therefore nearly symmetric in shape and very difficult to distinguish from the non s wave resonances.

The resonance at 103 kev ($\Gamma \approx 5.5$ kev) is quite symmetric in shape because it is located in the interference minimum of a resonance at 147.3 kev. The cross section is not zero below either resonance because of the presence of non s wave "noise".

Above 300 kev, the cross section is quite complicated. The resonance at 443.5 has been fitted as an s wave although it could probably be fitted equally well as a p wave. It was necessary to fit the resonance at 530 kev as an s wave in order to explain the shape of the cross section between 510 and 525 kev.

The resolution function for this fit was the same as for Ca^{42}.

Chromium

The cross section curves for the chromium isotopes are shown in Figures IV, V, and VI. The chromium samples were also furnished as oxides (Cr_2O_3) and were treated in the same manner as the calcium samples.

Cr^{50}. The resonances at 95.5, 130, 186.5 and 232.5 kev all exhibit

Figure 4. Chromium^{50} and Chromium^{54} 60-240 kev.

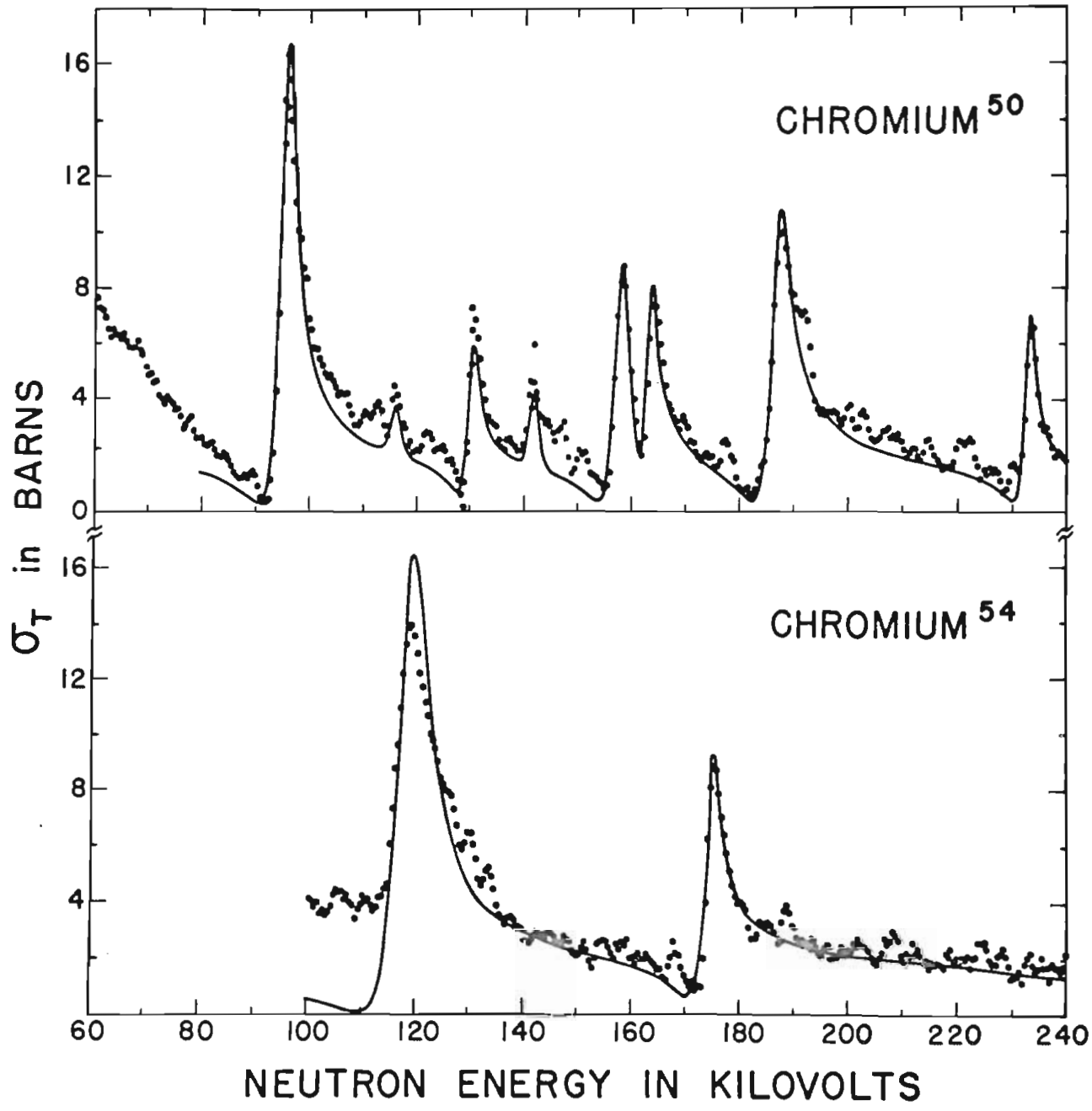
CHROMIUM 50
CHROMIUM 54
σ_T in BARNS
NEUTRON ENERGY IN KILOVOLTS
0
4
8
12
16
60
80
100
120
140
160
180
200
220
240

Figure 5. Chromium^{50} and Chromium^{54} 240-410 kev.

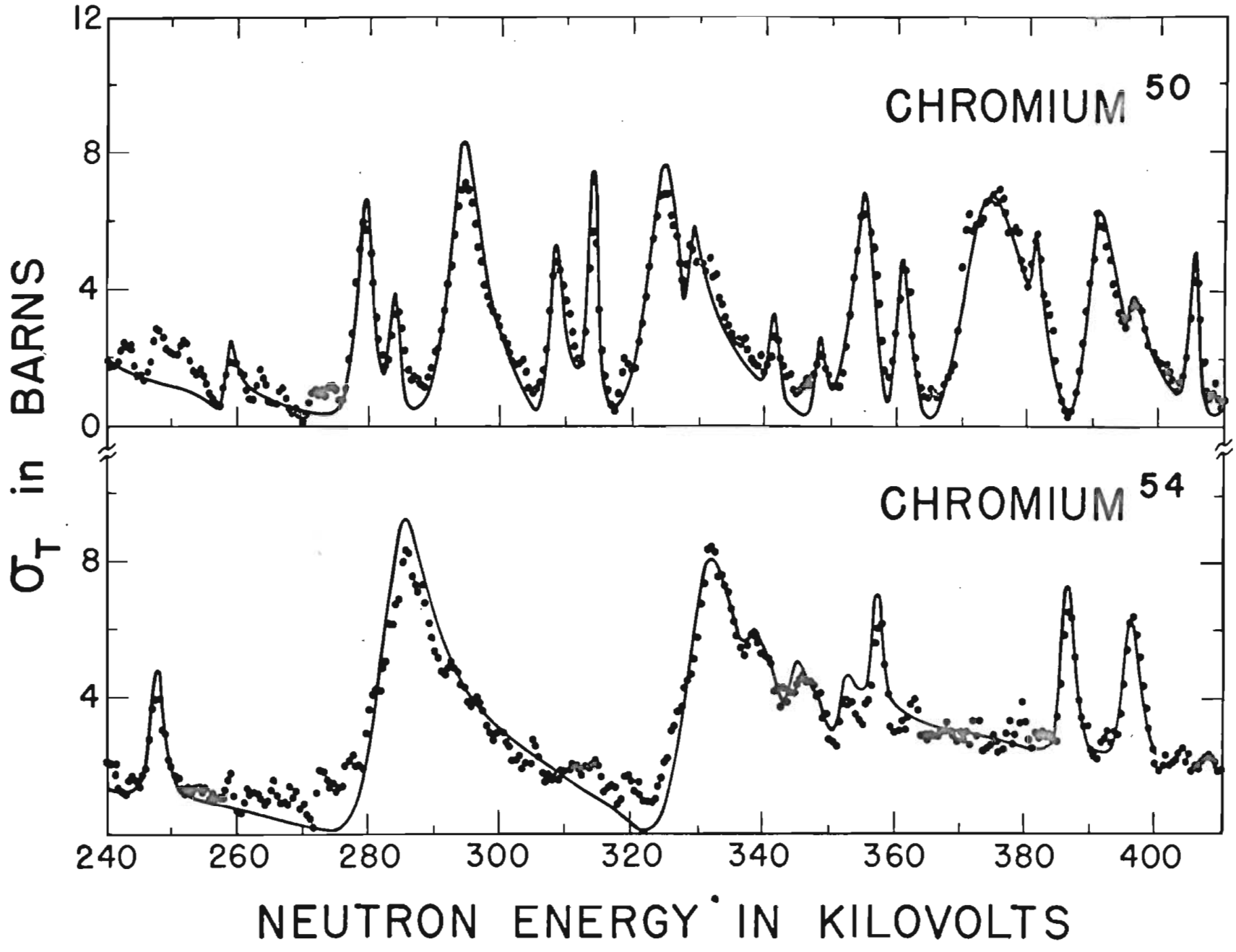
CHROMIUM 50
CHROMIUM 54
σ_T in BARNS
0
4
8
12
240
260
280
300
320
340
360
380
400
NEUTRON ENERGY IN KILOVOLTS

Figure 6. Chromium^{50} and Chromium^{54} 410-600 kev.

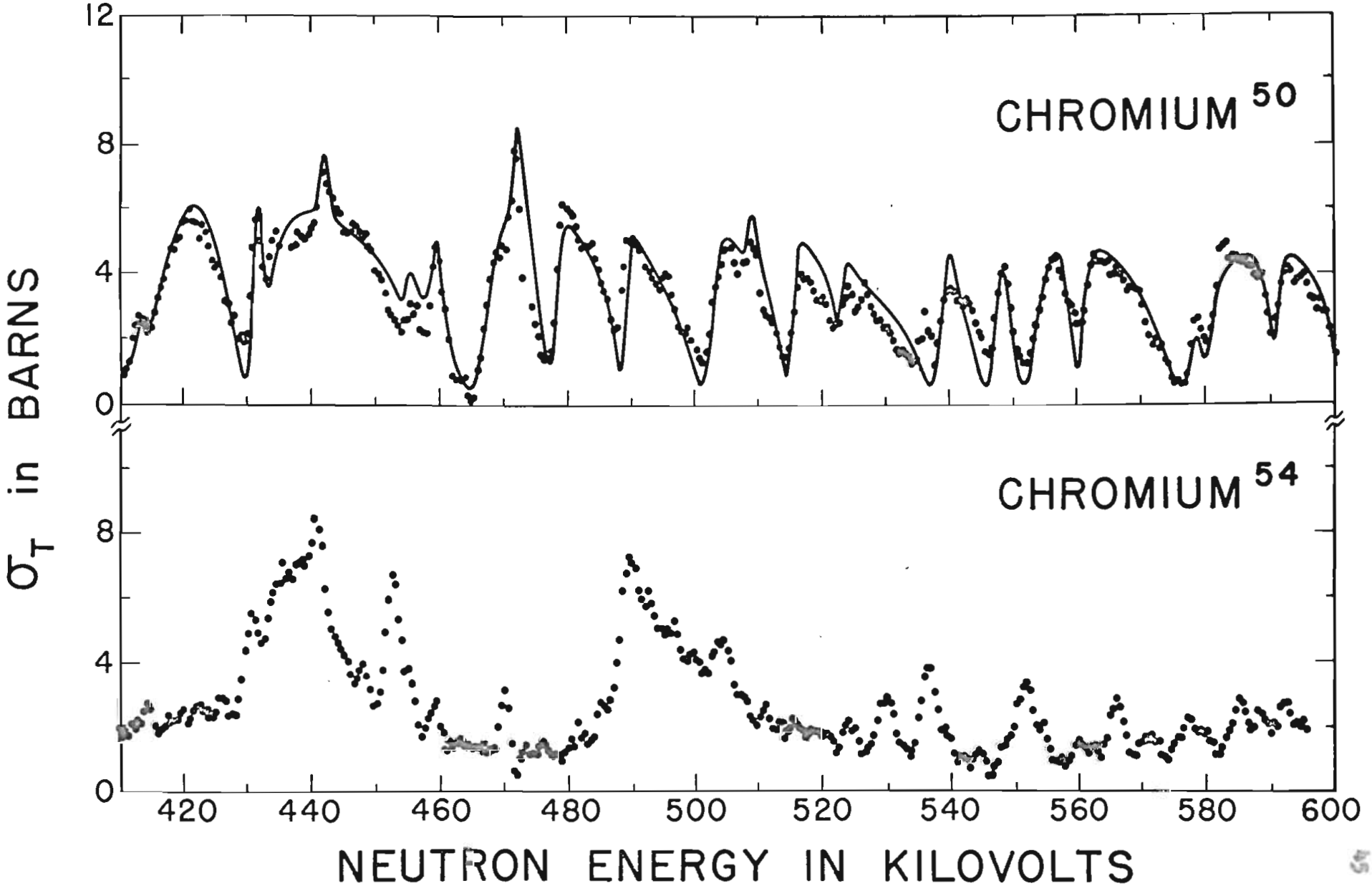
CHROMIUM 50
CHROMIUM 54
σ_T in BARNS
NEUTRON ENERGY IN KILOVOLTS
0
4
8
12
420
440
460
480
500
520
540
560
580
600

the typical s wave shape with pronounced interference minima and long tails. The other regions are much more complicated. The resonance at 157.5 kev is also an s wave in spite of its symmetric shape since it lies in the minimum of the resonance at 163.3 kev.

All of the resonances above 275 kev are strongly distorted by interference. Most of them have a nearly symmetric shape making them difficult to distinguish from higher angular momentum resonances. Neutron energy spread and small non s wave resonances tend to fill in the interference minima so that some resonances are improperly identified.

The resolution width used was 1.5 kev below 150 kev and 1.0 kev above.

Cr^{54}. Two samples containing Cr^{54} were furnished, one containing 1.8 grams of chromium metal, the other 4.2 grams of oxide (Cr_2O_3). Because of the small amount of chromium available and the presence of considerable oxygen, statistics on this data are relatively poor, particularly in the region of the oxygen resonance at 435 kev. Because of this, a fit to the data in this region was not attempted.

The structure at 108 kev also presented considerable difficulty in interpretation. There are evidently one or more fairly wide non s wave resonances involved as it is impossible to fit this region with a single s wave resonance. It was decided to fit the leading edge and peak with an s wave resonance and not to attempt to fit the surrounding region.

The resonances at 248, 357.5, 386.5 and 396.5 kev are all symmetric and have no indication of interference with potential scattering. For this reason, they have been interpreted as p wave resonances. They are not sufficiently well resolved to determine their J values.

Above 500 kev there are a number of small resonances for which it is impossible to determine angular momenta. The difficulty arises because of

the many non s wave resonances that tend to obscure any interference minima. The three small s wave resonances between 335 and 355 kev are distinguishable only because they happen to be situated on the tail of a much larger resonance. If they were located in a region of lower surrounding s wave cross section they would not be distinguishable from the non s wave "noise".

The resolution width used was 2.0 kev.

Nickel

The nickel isotopes were furnished as metallic powders with the exception of Ni^{64} which was fabricated at Oak Ridge National Laboratory. The use of isotopically pure metal improved the point scatter so that it was not necessary to smooth any of the nickel data. A resolution of 1.0 kev was used for all fits.

Ni^{58}. The data for Ni^{58} and Ni^{60} are shown in Figures VII, VIII and IX. The widths of the resonances below 210 kev are in agreement with the older data reported in Part VII. It was necessary to make small corrections in the resonance energies. This is partly due to drifts in the energy calibrations of the two runs and partly due to differences in the multilevel formulas employed. However, two new s wave resonances were discovered in this region at 136.5 and 167.5 kev. The resonance at 190.5 kev is almost symmetric because of its proximity to the wide resonance at 204.5 kev.

Above 300 kev, the cross section curve increases in complexity. This is due to the fact that $4\pi\lambda^2$ is getting smaller so that the s wave resonances are less conspicuous, while the non s wave resonances are becoming stronger.

Figure 7. Nickel^{58} and Nickel^{60} 50-250 kev.

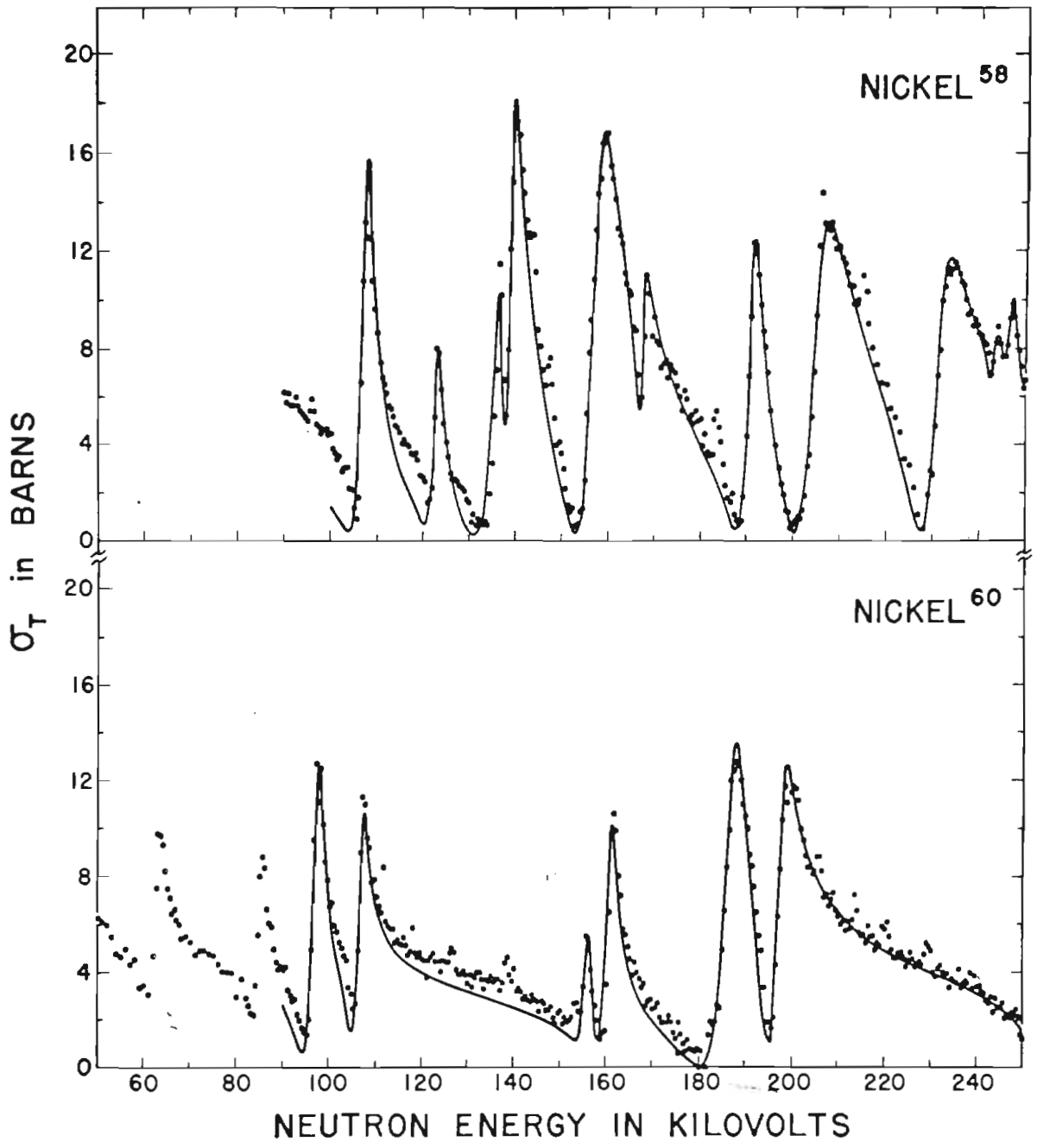
NICKEL 58
NICKEL 60
σ_T in BARNS
0
4
8
12
16
20
60
80
100
120
140
160
180
200
220
240
NEUTRON ENERGY IN KILOVOLTS

Figure 8. Nickel^{58} and Nickel^{60} 250-450 kev.

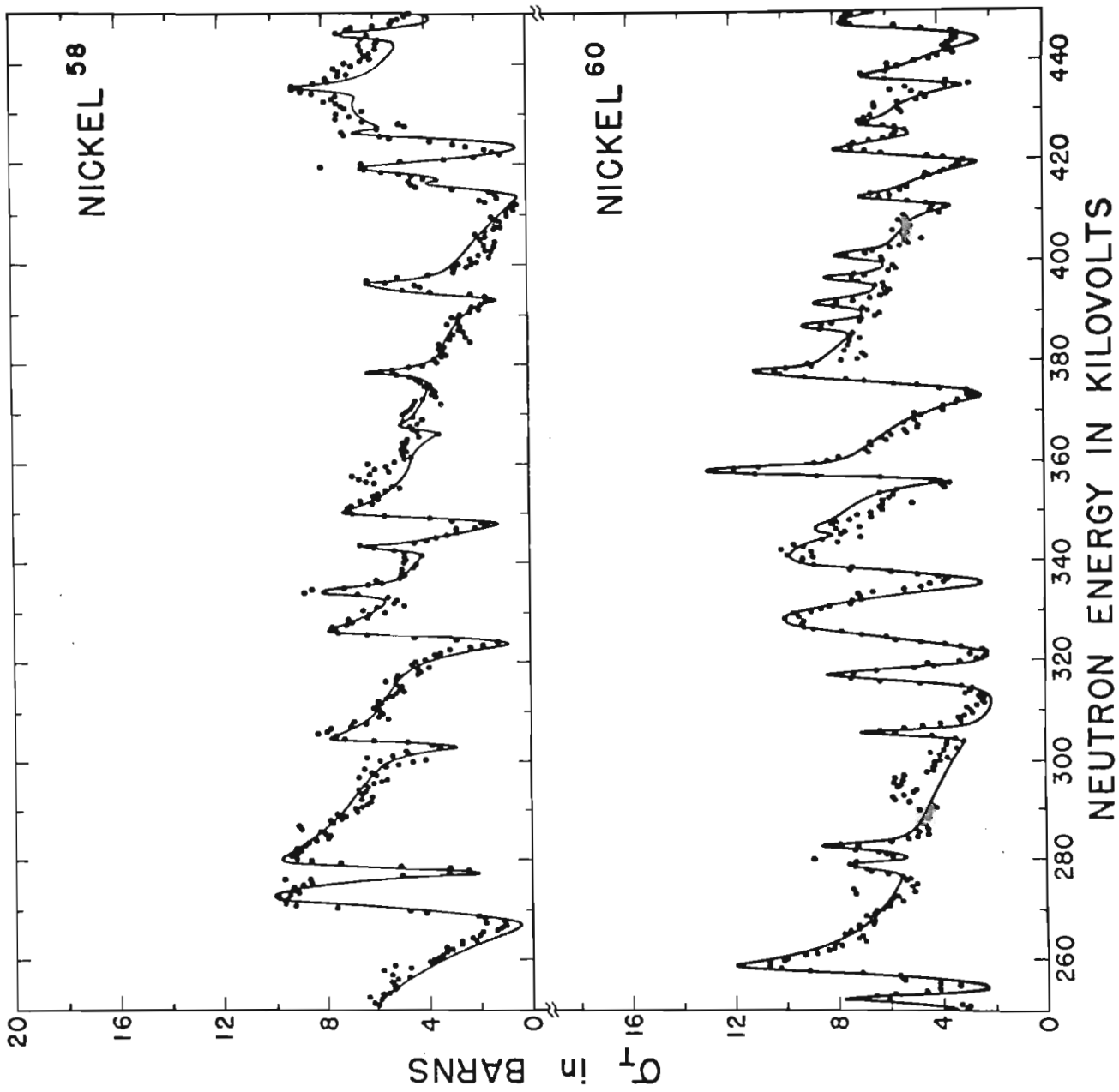
NICKEL 58
NICKEL 60
σ_T in BARNS
NEUTRON ENERGY IN KILOVOLTS
0
4
8
12
16
20
260
280
300
320
340
360
380
400
420
440

Figure 9. Nickel^{58} and Nickel^{60} 450-650 kev.

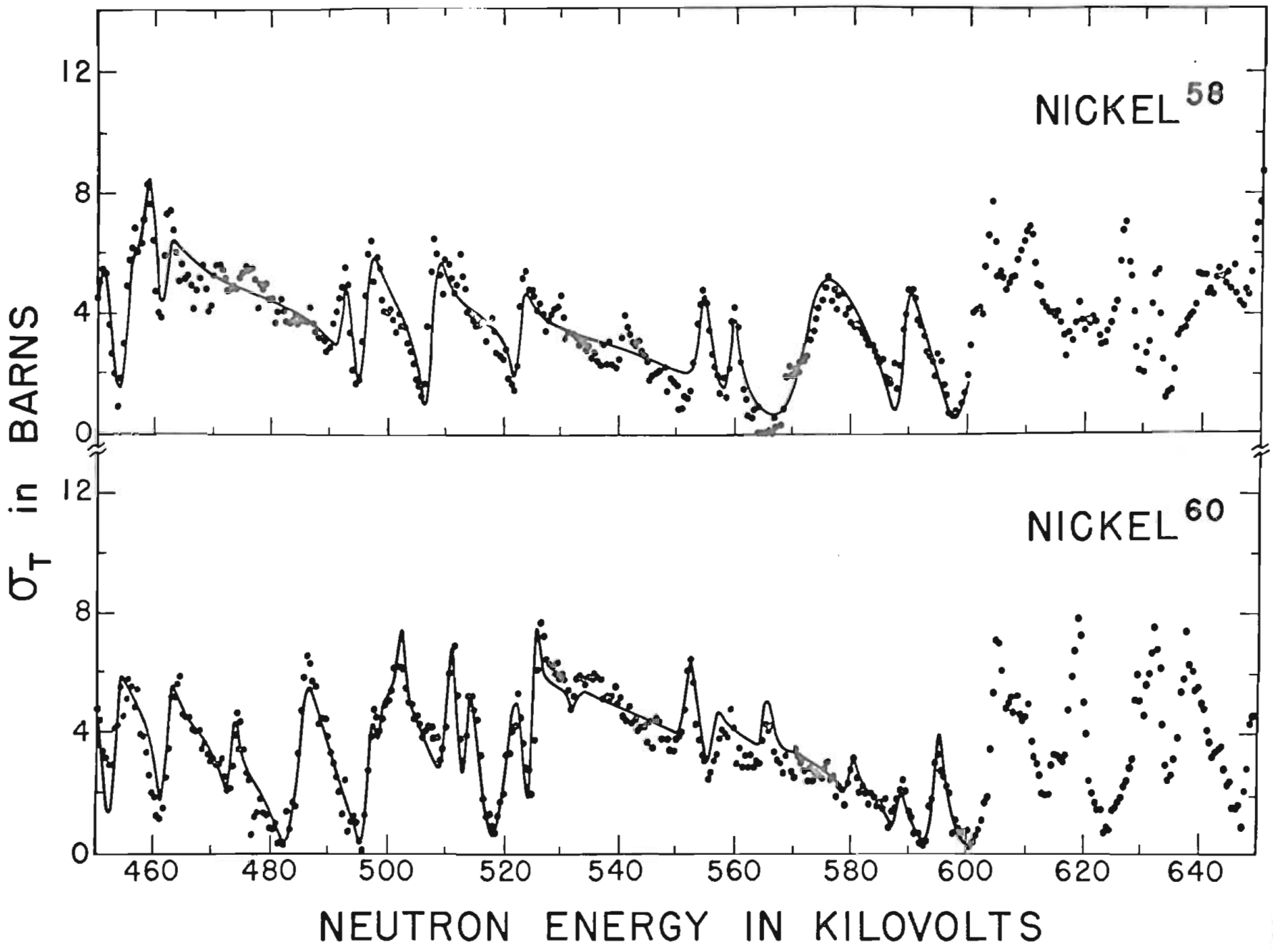
NICKEL 58
NICKEL 60
σ_T in BARNS
0
4
8
12
460
480
500
520
540
560
580
600
620
640
NEUTRON ENERGY IN KILOVOLTS

The high cross section in the region from 420 to 460 kev is probably due to the presence of a small amount of oxygen in the sample.

Ni^{60}. The resonance widths of the lower energy region agree with those reported in Part VII although small shifts in the resonance energies occurred again.

Most of the s wave resonances here are near enough to neighboring resonances that interference effects are important. The interference minimum of the resonance at 160 kev appears to be obscured by a p wave resonance at 156 kev. Several relatively large p wave resonances above 600 kev hide the underlying s wave structure so that a fit of this region is difficult if not impossible.

The structure at 358.5 kev has been interpreted as a p wave resonance (Γ = 0.3 kev and J = 3/2) sitting on the peak of an s wave resonance 1.0 kev wide. From 410 to 530 kev there are many s wave resonances a few kev wide which are greatly distorted by mutual interference.

Ni^{62}. The data for Ni^{62} and Ni^{64} are shown in Figures X, XI, and XII. Figure XIII shows the cross section for Ni^{62} taken at 160°. The dashed line was drawn to indicate the trend of the points and is not a multilevel fit. Three s wave resonances and one small non s wave resonance were found in this region as well as several other small peaks which may be real.

The pair of resonances near 100 kev furnish a beautiful example of two strongly interfering resonances, one 2.25 kev wide at 93.5 kev, the other 4.5 kev wide at 148.5 kev. The small resonance at 148.5 kev has been fitted with a width of 200 ev. Above 200 kev, the cross section becomes much more complicated although here the non s wave resonances are much more easily distinguished than in the calcium isotopes. A few of these resonances such as

Figure 10. Nickel^{62} and Nickel^{64} 50-250 kev.

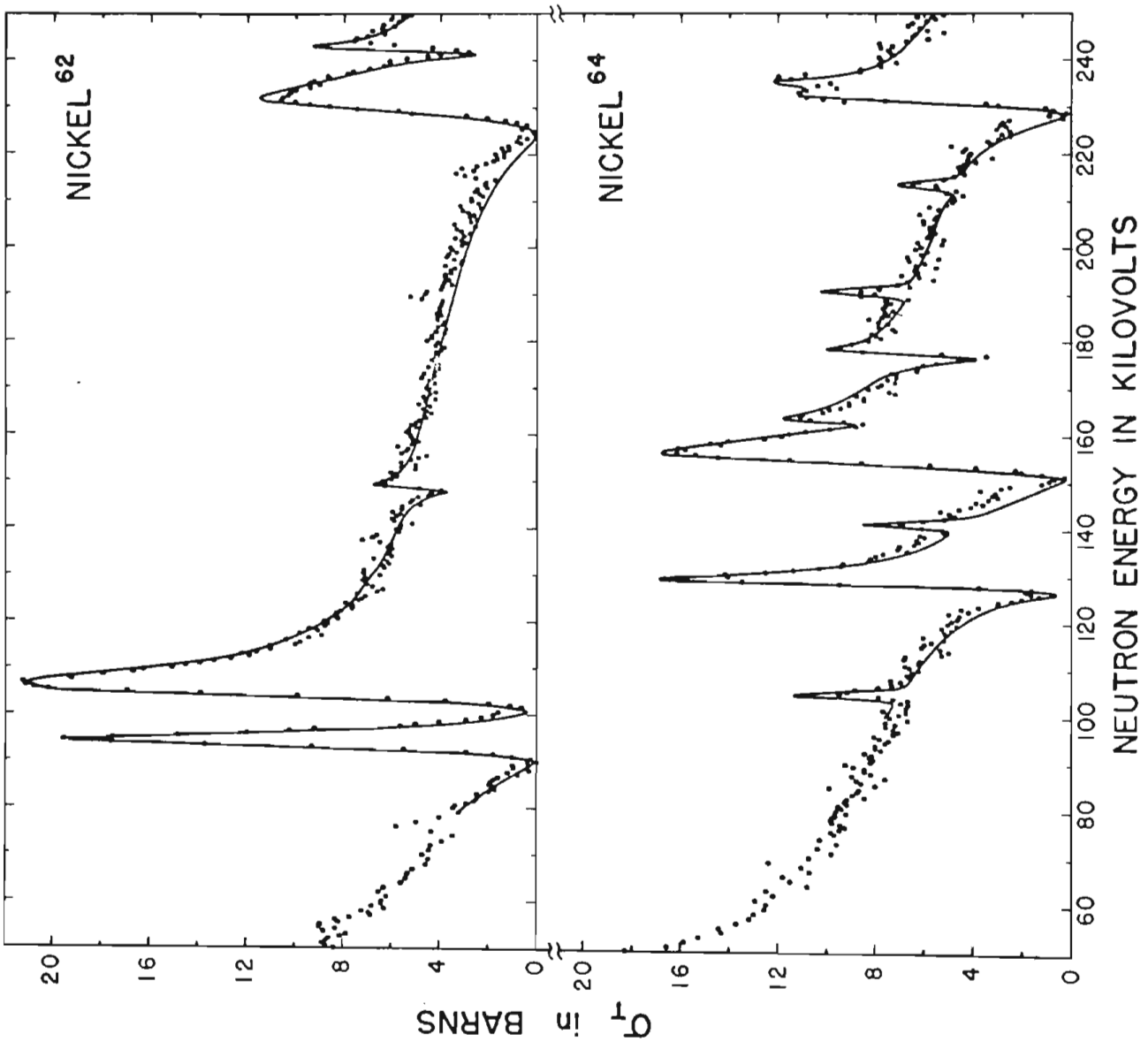
NICKEL 62
NICKEL 64
σ_T in BARNS
NEUTRON ENERGY IN KILOVOLTS
0
4
8
12
16
20
60
80
100
120
140
160
180
200
220
240

Figure 11. Nickel^{62} and Nickel^{64} 250-450 kev.

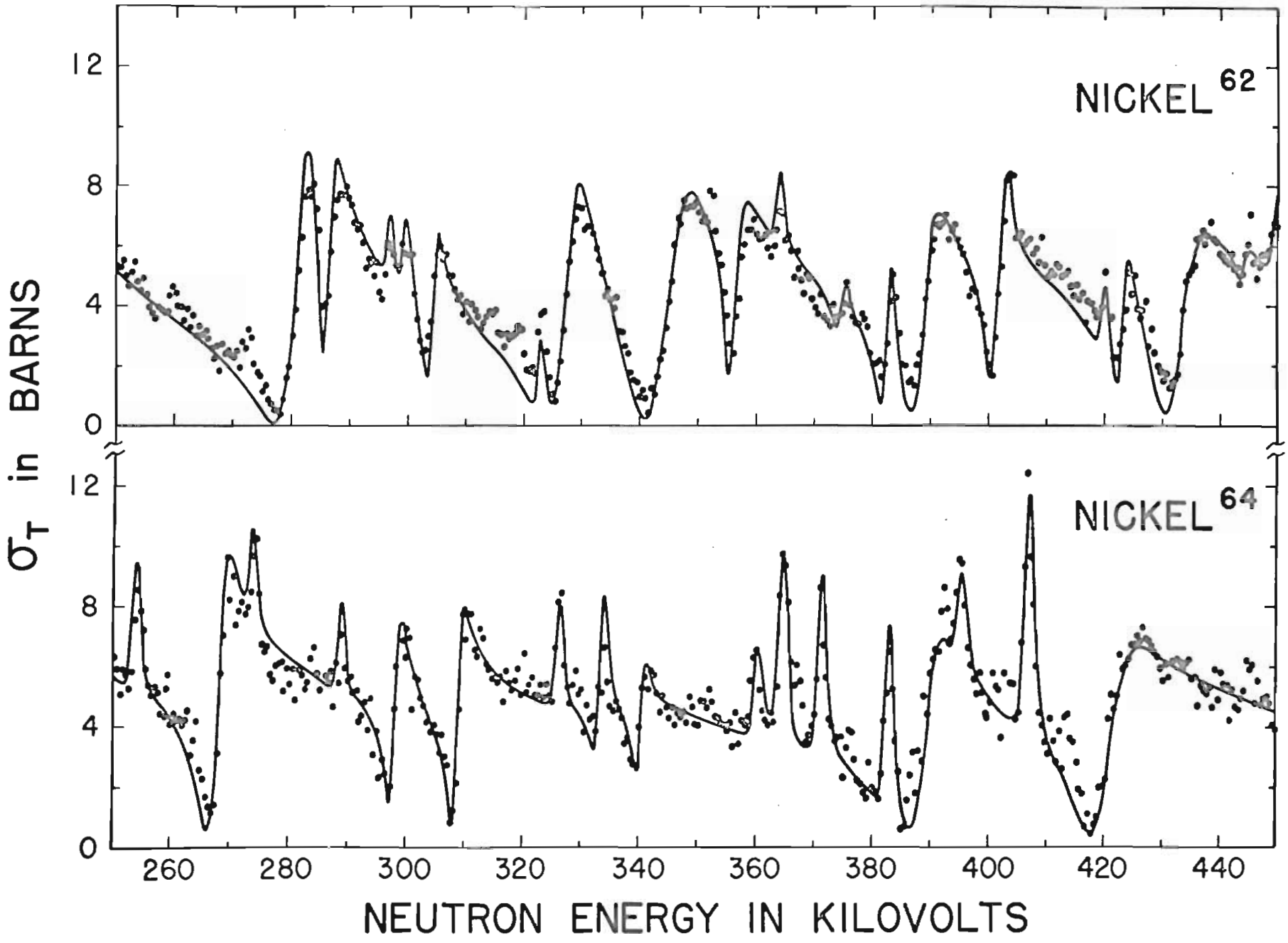
NICKEL 62
NICKEL 64
σT in BARNS
0
4
8
12
260
280
300
320
340
360
380
400
420
440
NEUTRON ENERGY IN KILOVOLTS

Figure 12. Nickel^{62} and Nickel^{64} 450-650 kev.

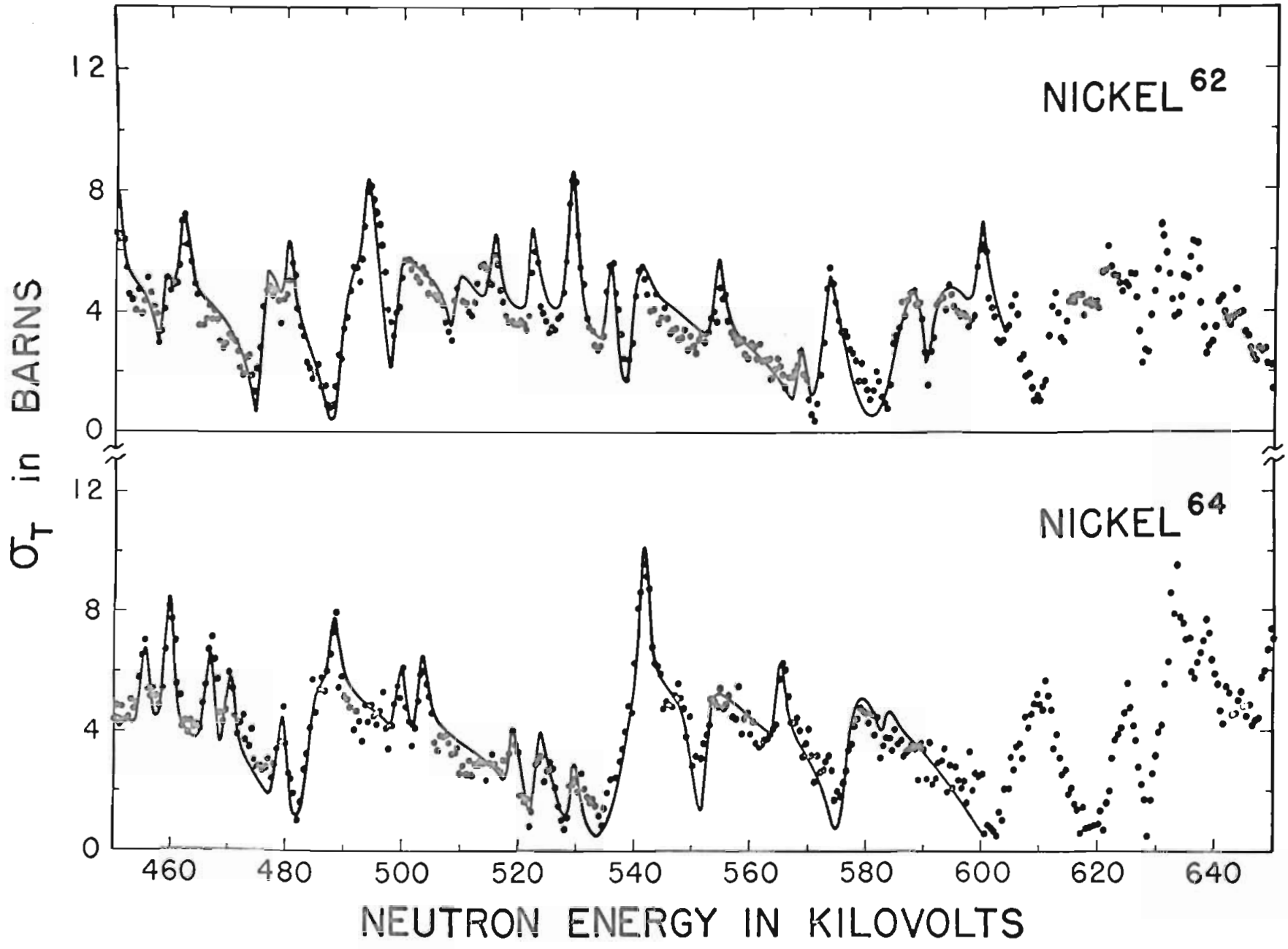
NICKEL 62
NICKEL 64
σT in BARNS
0
4
8
12
460
480
500
520
540
560
580
600
620
640
NEUTRON ENERGY IN KILOVOLTS

Figure 13. Michel[62] 3-81 kev.

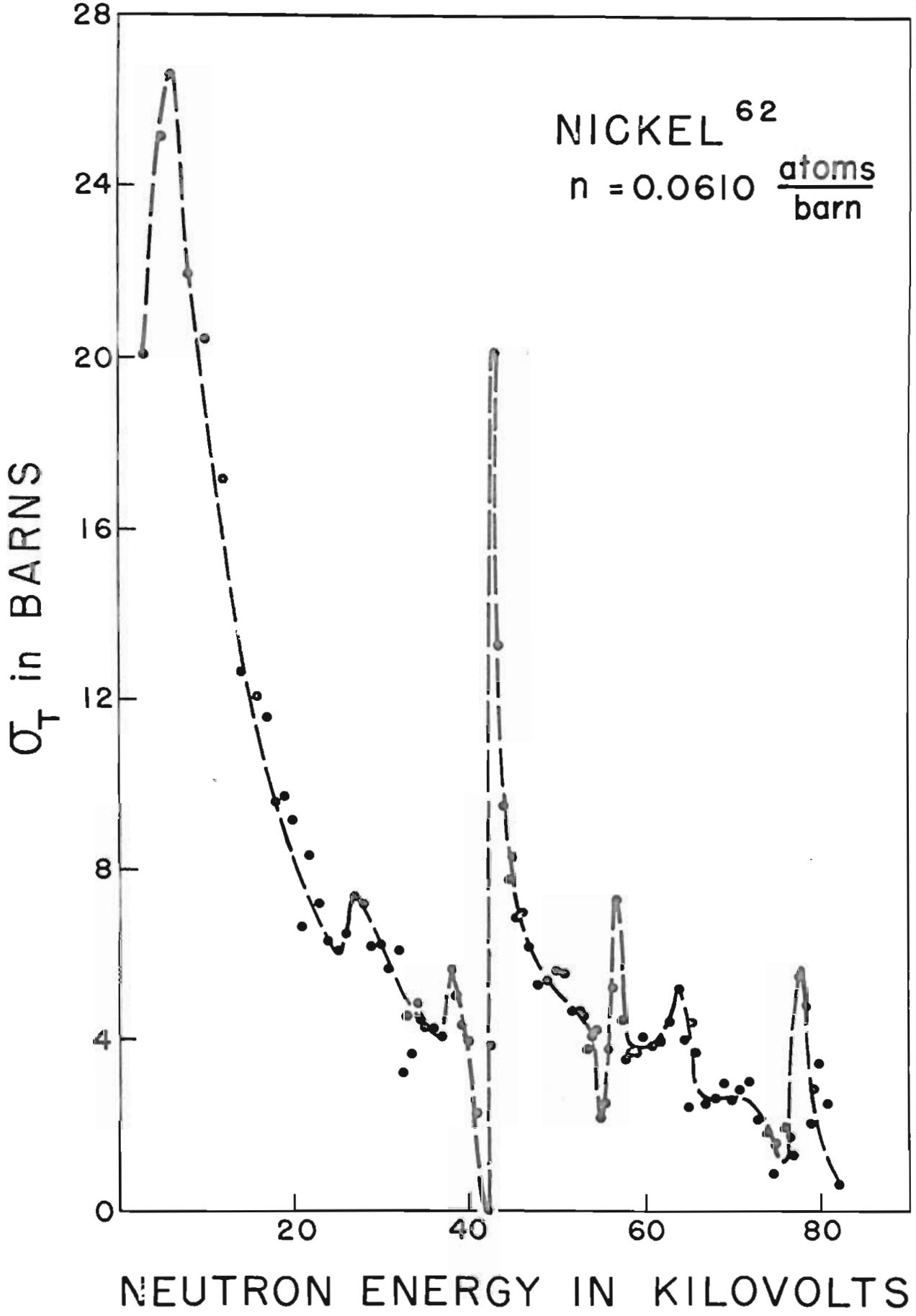
NICKEL 62
n = 0.0610 atoms/barn
σT in BARNS
0
4
8
12
16
20
24
28
20
40
60
80
NEUTRON ENERGY IN KILOVOLTS

the ones at 404, 494 and 529 kev are wide enough to permit a determination of the J values of the levels.

Ni^{64}. This sample was furnished as a small disk, 1 cm. in diameter and weighing only 4 grams. Because of the thinness of the sample, the point scatter is slightly worse than the other nickel isotopes.

The cross section exhibits more non s wave resonances than the other nickel isotopes but most of them can be clearly distinguished. Several of these such as those at 365, 371.5, 383 and 407 kev are wide enough to determine J unambiguously.

CHAPTER IV

INTERPRETATION

In order to compare the behaviour of the average level spacings with the predictions of various nuclear models, the data on the nuclides just discussed have been combined with those reported in Part VIII.

Width and Spacing Distributions

There are too few levels observed for an investigation of the widths and spacings of each compound nucleus separately. However, by calculating the ratios $x = \Gamma_n^\circ / \bar{\Gamma}_n^\circ$ and $y = D/\bar{D}$, we can combine the data for all the nuclei observed. This gives us a total of 283 reduced widths $\Gamma_n^\circ = \Gamma/\sqrt{E}$ and 271 local spacings (D).

Figure XIV gives a histogram of $\Gamma_n^\circ/\bar{\Gamma}_n^\circ$ fitted with the Porter-Thomas distribution (Porter and Thomas, 1956)

$$P(x) = (2\pi x)^{-\frac{1}{2}} \exp(-x/2) \ . \qquad (1)$$

Agreement is excellent except at the ends of the range. A close agreement for the wide resonances would not be expected since so few were observed we do not have a statistically significant sample.

If we accept the Porter-Thomas distribution as correct, we can use Figure XIV to estimate the number of levels missed. The fit indicates that

Figure 14. Distribution of Reduced Widths.

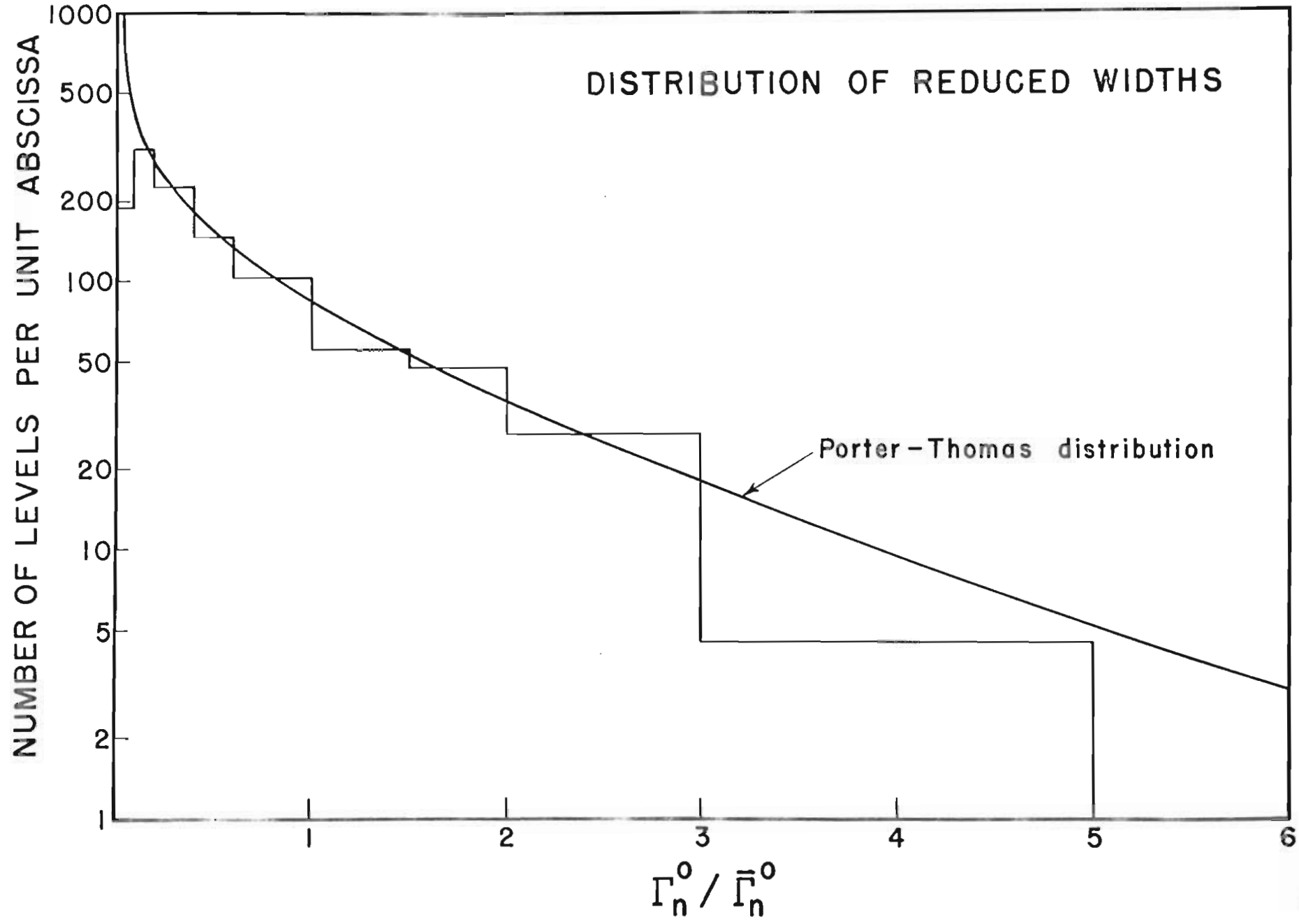
DISTRIBUTION OF REDUCED WIDTHS
NUMBER OF LEVELS PER UNIT ABSCISSA
1000
500
200
100
50
20
10
5
2
1
Porter-Thomas distribution
1
2
3
4
5
6
$\Gamma_n^o / \bar{\Gamma}_n^o$

very few levels wider than 1/10 of the average reduced width were missed but that a relatively large number of resonances narrower than this were not found. This corresponds to an actual width of approximately 250 ev at neutron energies of 200 to 300 kev. Integrating the Porter-Thomas distribution up to $x = 1/10$ and comparing with the number of resonances observed in this range we find that we missed approximately 65 resonances or 19% of the total.

These small resonances are likely to be noticed only when they lie on the tail of a wider resonance but even there they may be obscured by small non s wave resonances. If a small s wave resonance lies near the interference minimum of a larger one, it will be symmetric in shape and cannot be distinguished from a higher angular momentum resonance. On the other hand, some non s wave resonances in this position were probably identified incorrectly as s waves. Since no fit was attempted on the smaller non s wave resonances, it is unlikely that many were misinterpreted.

Figure XV is a histogram of the ratios of observed level spacings to the average level spacing $(\overline{D})$. The solid curve is the Wigner distribution (Wigner, 1957)

$$P(y) = \frac{\pi y}{2} \exp(-y^2/4) \qquad (2)$$

normalized to the same total area as the histogram. Here the agreement is relatively poor. According to the Wigner distribution we have seen too few spacings less than twice the average spacing and too many wide spacings. In addition, there is a small discrepancy between $y = 0$ and 0.75, but it disappears if we renormalize the Wigner distribution (dashed curve, Figure XV) taking into account the missed levels indicated by the Porter-Thomas distribution. If the excess of wide spacings observed is due to the missed

Figure 15. Distribution of Level Spacings.

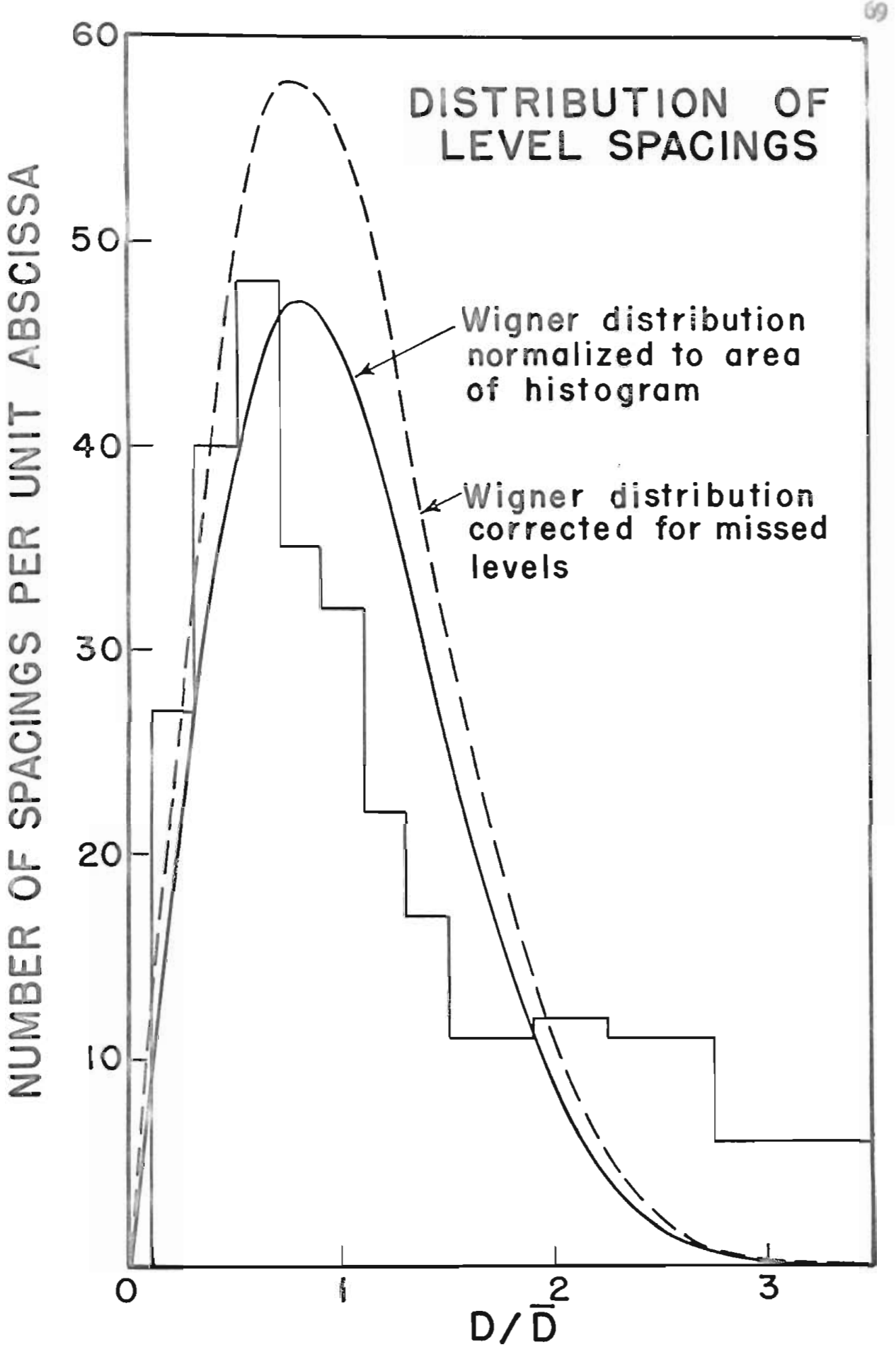
DISTRIBUTION OF LEVEL SPACINGS
NUMBER OF SPACINGS PER UNIT ABSCISSA
60
50
40
30
20
10
0
1
2
3
D/D̄
Wigner distribution normalized to area of histogram
Wigner distribution corrected for missed levels

levels, the area between the histogram and the curve from y = 0.75 to 1.9 should be twice the area of the histogram above the tail of the curve for y above 1.9, since splitting one large spacing results in two smaller spacings. The observed ratio is 2.4. Assuming that the excess of wide spacings is due to missed resonances, we find that we must have missed approximately 40 resonances. Considering the accuracy of these calculations, this is in excellent agreement with the number of resonances missed according to the Porter-Thomas distribution. We conclude that the Wigner and Porter-Thomas distributions together explain the data very well.

Average Level Spacings, Rosenzweig's Model

From the experimental data, we calculate

$$D_o(B) = \frac{2\Delta E(2I+1)}{n} = 2\bar{D}\,(2I+1) \qquad (3)$$

where I is the spin of the target nucleus and n is the number of s wave resonances observed in the energy interval ΔE. Since all of the nuclei dealt with here are even-even, $D_o(B)$ is just twice the observed level spacing.

We then normalize the spacings to an excitation energy of 6 mev using the relation (valid when B-6 is small)

$$D_o(6) = D_o(B) \exp\left(\frac{B-6}{t}\right) \qquad (4)$$

where B is the excitation energy, U, of the compound nucleus at the neutron escape energy and t is the nuclear temperature. Since little data on nuclear temperatures in this region was available, we used the same average value (1.2) as in Part VIII. This same average nuclear temperature also follows from the Fermi gas model level density coefficients measured by Kapadia(1963)

from neutron inelastic scattering. Table IV lists Z, N, N-Z = T, energy range, n, $D_o(S)$ and $D_o(S)$ for the data reported here, the data of Part VIII and data for the even-even isotopes of zinc, germanium and selenium which have been measured at Oak Ridge National Laboratory by Muenzer, Nishimura and Good (1961).

Figure XVI shows a typical shell model level scheme. Part VIII compared the observed spacings with Rosenzweig's model (Rosenzweig, 1957) assuming that the $f^{7/2}$ subshell is isolated. When we added the data for the newly measured calcium isotopes, we found that the points fell below the theoretical curve by a factor of three to five. This poor agreement and the large s wave level spacing of S^{32} has led us to apply Rosenzweig's model assuming that at these excitation energies, the $d^{3/2}$ subshell overlaps the $f^{7/2}$ subshell, thus closing a major shell at 16 nucleons rather than 20.

Rosenzweig's theory gives for the ratio of spacings of two isotopes:

$$\frac{D_b}{D_a} = \exp \frac{2q^{\gamma}}{4gU^2}\left[(n_b - \frac{g}{2})^2 - (n_a - \frac{g}{2})^2\right] \qquad (5)$$

where

$$q = \left[\frac{2\pi^2}{3}(\frac{g}{\gamma} + \frac{d}{\delta})\right]^{\frac{1}{4}}$$

and n_a, n_b are the number of nucleons in the unfilled subshells,

g,d are neutron and proton subshell degeneracies,

γ,δ are the energy gaps between subshells for neutrons, and protons respectively and

U is the excitation energy.

An analogous expression can be derived for a pair of isotones.

We have sufficient data available to compare ratios of spacings for sets of nuclei with the same neutron excess, T, if we make the further assumption that $g = d$ and $\gamma = \delta$.

Table IV. Average Level Spacings

Nucleus	Z	N	T	Energy Range (kev)	n	D_0(B) (kev)	D_0(6) (kev)
S^{32}	16	16	0	0-635	3	280	520
Ca^{40}	20	20	0	0-635	13	98	1196
Ca^{42}	20	22	2	100-650	22	50	244
Ca^{44}	20	24	4	100-600	16	63	205
Ti^{46}	22	24	2	40-340	11	60	258
Ti^{48}	22	26	4	0-365	17	44	253
Ti^{50}	22	28	6	37-307	4	246	324
Cr^{50}	24	26	2	95-620	36	29	384
Cr^{52}	24	28	4	50-630	14	88	448
Cr^{54}	24	30	6	100-600	10	100	98
Fe^{54}	26	28	2	0-506	20	50	910
Fe^{56}	26	30	4	0-645	22	58	183
Ni^{58}	28	30	2	0-600	27	45	535
Ni^{60}	28	32	4	0-600	34	35	282

Table IV (continued)

Nucleus	Z	N	T	Energy Range (kev)	n	$D_0(B)$ (kev)	$D_0(6)$ (kev)
Ni^{62}	28	34	6	90-600	28	36	72
Ni^{64}	28	36	8	100-600	19	53	73
Zn^{64}	30	34	4			6.0	32
Zn^{66}	30	36	6			9.0	22
Zn^{68}	30	38	8			17	24
Ge^{70}	32	38	6			2.4	7.0
Ge^{72}	32	40	8			4.4	6.5
Ge^{74}	32	42	10			17	24
Ge^{76}	32	44	12			16	14
Se^{76}	34	42	8			2.4	7.8
Se^{78}	34	44	10			8.0	12
Se^{80}	34	46	12			8.0	15
Se^{82}	34	48	14			14	25

Figure 16. Shell Model Level Diagram.

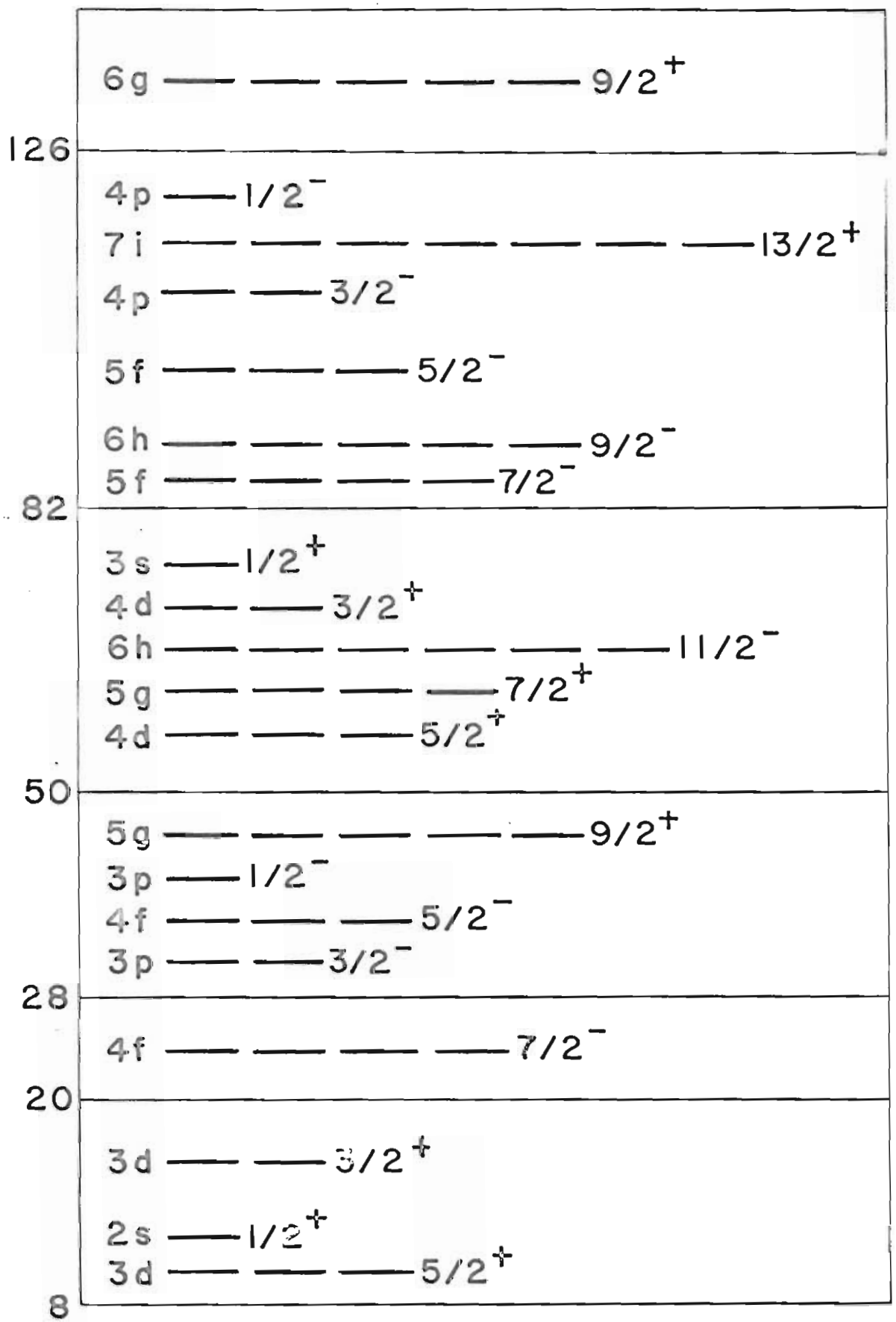
6g ——— 9/2+
126
4p —— 1/2−
7i ——— 13/2+
4p —— 3/2−
5f ——— 5/2−
6h ——— 9/2−
5f ——— 7/2−
82
3s —— 1/2+
4d —— 3/2+
6h ——— 11/2−
5g ——— 7/2+
4d ——— 5/2+
50
5g ——— 9/2+
3p —— 1/2−
4f ——— 5/2−
3p —— 3/2−
28
4f ——— 7/2−
20
3d —— 3/2+
2s —— 1/2+
3d ——— 5/2+
8

Assuming that the shell comprises those nucleons between 16 and 28, we have g and d = 12. Since the spacings have all been corrected to an excitation energy of 6 mev we put U = 6 mev. Then Rosenzweig's model predicts:

$$\frac{D_b}{D_a} = \exp K \left[(n_b - 6)^2 - (n_a - 6)^2 \right]$$

where (6)

$$K = \frac{\pi}{12} \left(\frac{\gamma}{6} \right)^{\frac{1}{2}} .$$

We calculate K from the ratios of spacings for the three nuclei with T = 4 and the three with T = 2 using only those nuclei with N and Z $\leq$ 28. We get an average value of K = 0.0254 which leads to γ = 0.56 mev. The reason for this apparently low value of γ has been discussed in Part VIII.

We apply the same procedure to those nuclei with N and Z between 28 and 50. Here, g = 22 giving

$$\frac{D_b}{D_a} = \exp K' \left[(n_b - 11)^2 - (n_a - 11)^2 \right] . \qquad (7)$$

We determine K' in the same manner as K.

Following the procedure of Part VIII we have corrected the spacings for those nuclei with N $\leq$ 28 to the spacings for a half filled subshell of protons (Z = 22) using Eq. (6). We have plotted the resulting spacings as a function of N in Figure XVII, using a different symbol for each T. We have done the same thing for the other nuclei with Z > 28, normalizing the spacings so that they match the lighter nuclei at N = 28. The theoretical curves are obtained from Eqs. (6) and (7).

We see that the agreement is excellent for those nuclei with T = 2 and 4 and N $\leq$ 28, and, in addition, there is a clear dependence upon T with the points with higher T lying lower. If we assume an exponential dependence

Figure 17. Average Level Spacings Compared with Rosenzweig's Model.

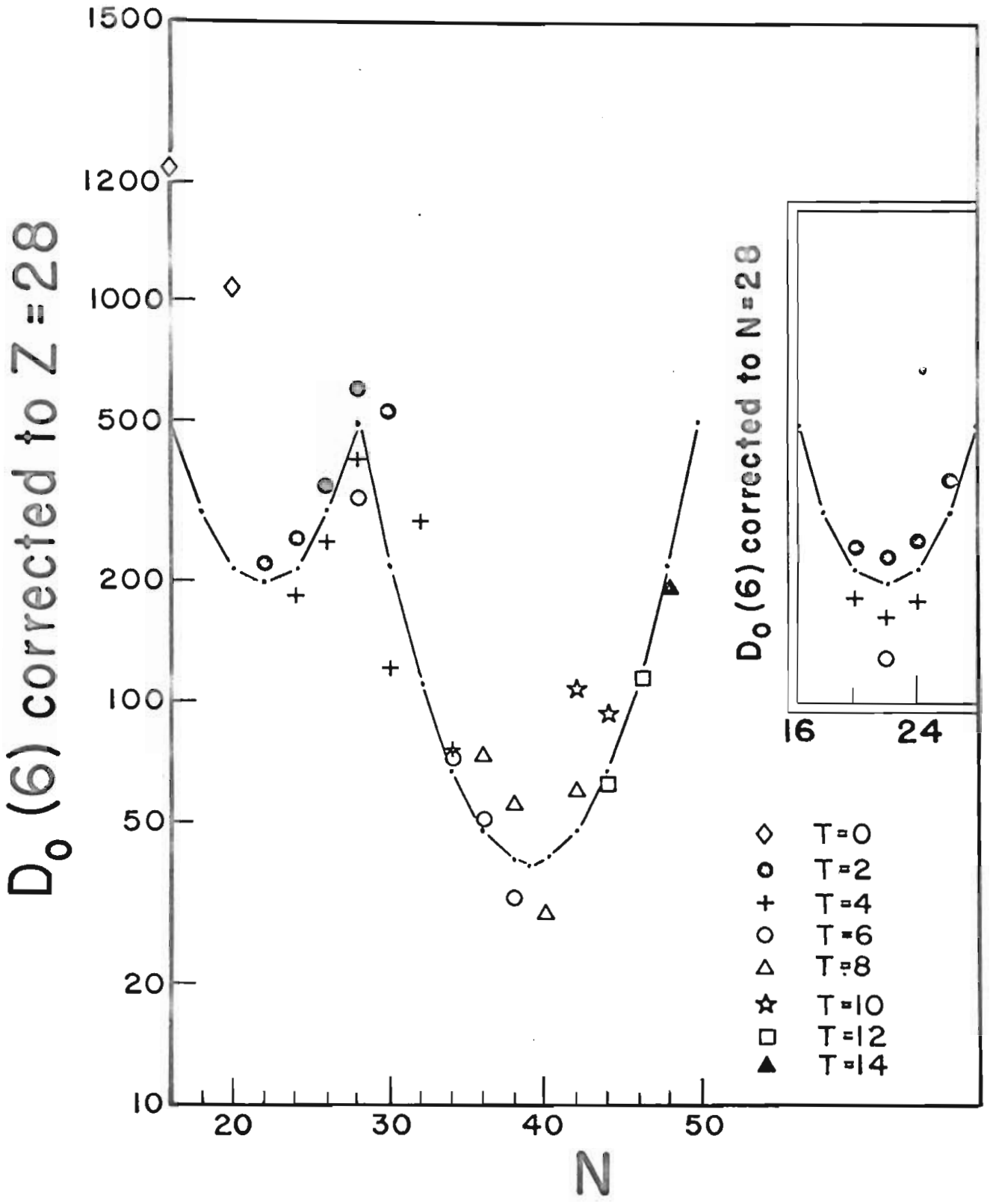
1500
1200
1000
500
200
100
50
20
10
20
30
40
50
N
D_o (6) corrected to Z = 28
D_o (6) corrected to N = 28
16
24
T = 0
T = 2
T = 4
T = 6
T = 8
T = 10
T = 12
T = 14

on neutron excess as in Parts VI and VIII, we get 0.17 for the coefficient of T in the exponential. This is less than the value of 0.27 obtained in Part VIII. This is due to the different correction for the subshell effect employed.

The fit for Z > 28 is not as good and there is no consistent effect with T. This may be partly due to the fact that the Oak Ridge data is based on a smaller energy range and fewer resonances so that statistics on each point are not as good. But, there is reason to believe that the neutron excess effect is most important for small values of T since the points for the T = 0 nuclei, S^{32} and Ca^{40} lie far above the curve.

The inset in Figure XVII, page 78, shows the data for N ≤ 28 corrected with Eq. (6) to N = 22 plotted as a function of Z and compared with Rosensweig's model. Again we get an excellent agreement for T = 2 and 4 with the T = 4 points consistently lying lower.

We note that the difficulty with Cr^{50} reported in Part VIII was due to the quality of the data and that the new higher resolution data indicates a much smaller level spacing which agrees better with the calculated curve.

Average Level Spacing, Newson and Duncan Model

A simpler method of predicting average level spacings is that of Newson and Duncan (1959). Referring to Figure XVI, page 75, we count the number of ways of distributing pairs of neutrons in the unfilled shell among the levels of that shell, assuming that each subshell is completely degenerate. We denote this number by n_N. We obtain n_Z in a similar manner by counting the possible configurations of proton pairs. The level spacing should then be proportional to $(n_N\ n_Z)^{-1}$.

For the purpose of comparing this theory to our data, we have made the counts assuming again that a shell is closed at 16 rather than 20. Figure XVIII shows the results. We have made a separate plot for each set of nuclei with the same neutron excess so that it is unnecessary to make a correction for the dependence of the level spacing on neutron excess. The solid curve is given by const. $(n_N\ n_Z)^{-1}$. In general, the agreement is excellent except for the T = 0 nuclei but even these follow the general trend of the curve. For each T, there is a maximum in the level spacing whenever N or Z is 28 as predicted by the theoretical curve.

A similar and apparently more realistic count of pair configuration states can be carried out under the assumption that each subshell is not degenerate. Here, the n's are just the binomial coefficients since each fermion level will hold only one pair. This method leads to a peak to valley ratio in the spacings that is much too high so that agreement with the experimental data is poor. Newson and Gibbons (1963) have discussed the implications of the greater success of the configuration count over the configuration state count.

Average Level Spacings, Newton's Model

While this model (Newton, 1956) is known to give good agreement with experimental measurements of spacings of heavy elements, it deviates badly below N = 40 and cannot be used for our data--at least as the theory was originally proposed.

Figure 13. Average Level Spacings Compared with the Newson and Duncan Model.

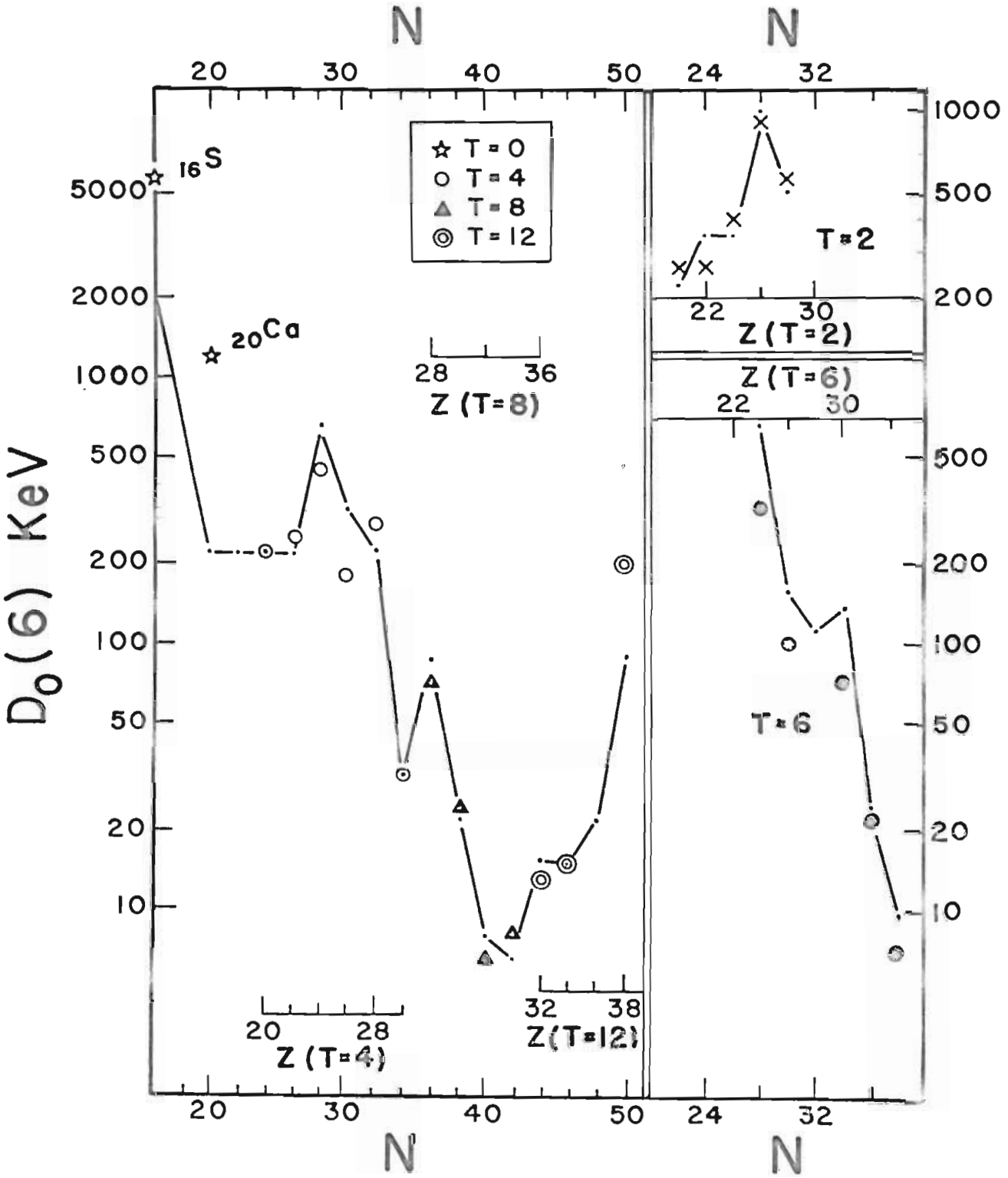
N
N
20
30
40
50
24
32
T = 0
T = 4
T = 8
T = 12
^{16}S
^{20}Ca
28
36
Z (T=8)
T=2
22
30
Z (T=2)
Z (T=6)
22
30
T=6
$D_o(6)$ KeV
5000
2000
1000
500
200
100
50
20
10
1000
500
200
100
50
20
10
20
28
Z (T=4)
32
38
Z(T=12)
N'
N

Conclusions

We have compared our experimental level spacings with the predictions of two different models and obtained good agreement with each. The two theories, while quite different in detail, are both based on a shell model level scheme. We can conclude that the observed level spacings are strongly influenced by the shell structure of the nucleus in that the spacings tend to peak at the magic numbers and have minima when N and Z are at the middle of a shell but the models are in need of considerable refinement. For instance, neither in its present form can predict the nuclear temperature. In addition, both models are based on enormously simplified assumptions so that one should not expect even as good an agreement as we have observed.

LIST OF REFERENCES

LIST OF REFERENCES

R. C. Block, unpublished Ph.D. dissertation, Duke University, 1956.

C.D. Bowman, unpublished M.A. thesis, Duke University, 1958.

C.D. Bowman, unpublished Ph.D. dissertation, Duke University, 1961.

C.D. Bowman, E.G. Bilpuch and H.W. Newson, Ann. Phys. 17, 319 (1962).

B. Chern, unpublished M.A. thesis, Duke University, 1954.

P.W. Crutchfield, unpublished M.A. thesis, Duke University, 1955.

J.H. Gibbons, unpublished Ph.D. dissertation, Duke University, 1954.

C.J. Kapadia, unpublished M.A. thesis, Duke University, 1963.

F.P. Karriker, unpublished M.A. thesis, Duke University, 1956.

H. Marshak, unpublished Ph.D. dissertation, Duke University, 1956.

H. Muenzer, K. Nishimura and W.M. Good, Bull. Am. Phys. Soc. II, 6, 251 (1961).

H.W. Newson, E.G. Bilpuch, F.P. Karriker, L.W. Weston, J.R. Patterson and C.D. Bowman, Ann. Phys. 14, 365 (1961).

H.W. Newson and M.M. Duncan, Phys. Rev. Letters 3, 45 (1959).

H.W. Newson and J.H. Gibbons, Fast Neutron Physics, Part II, J.B. Marion and J.L. Fowler, eds.,(Interscience, New York, 1963).

T.D. Newton, Can. J. Phys. 34, 804 (1956).

P.B. Parks, H.W. Newson and R.M. Williamson, Rev. Sci. Instr. 29, 834 (1958).

J.R. Patterson, unpublished Ph.D. dissertation, Duke University, 1955.

C.E. Porter and R.G. Thomas, Phys. Rev. 104, 483 (1956).

R.H. Rohrer, unpublished Ph.D. dissertation, Duke University, 1954.

N. Rosenzweig, Phys. Rev. 108, 817 (1957).

R.G. Smith, unpublished M.A. thesis, Duke University, 1955.

A.L. Toller, unpublished Ph.D. dissertation, Duke University, 1954.

E.P. Wigner, Proceedings of the International Conference on Neutron Interactions with Nuclei, Columbia University, TID-7547, p. 49 (1957).

The series of papers in Annals of Physics are:

Part I, 8, 194 (1959); Part II, 8, 211 (1959); Part III, 8, 223 (1959); Part IV, 8, 250 (1959); Part V, 14, 346 (1961); Part VI, 14, 365 (1961); Part VII, 14, 387 (1961); Part VIII, 17, 319 (1962); Part IX, X and XI to be published.

Part XIa, 37, 367 (1966);

BIOGRAPHY

John Alden Farrell

Born: December 25, 1935, Fort Worth, Texas

Education:

B.A. Texas Christian University 1959

Positions:

Teaching Assistant	Duke University	1959-1960
Du Pont Postgraduate Teaching Assistant		1960-1961
Duke Woodrow Wilson Fellow		1961-1962
Research Assistant	Duke University	1962-1964
Part Time Instructor	Duke University	1963

Abstracts:

Neutron Total Cross Sections of Lead Isotopes in the Kilovolt Region (with Kyker, Bilpuch and Newson), Bull. Am. Phys. Soc. II, 7, 289 (1962).

High Resolution Measurement of the $A^{40}(p,n)K^{40}$ Relative Cross Section (with Bilpuch, Parks, Beard, Kyker and Newson), Bull. Am. Phys. Soc. II, 8, 48 (1963).

S Wave Strength Functions near Mass Number 50 (with Bilpuch, Bowman and Newson), Bull. Am. Phys. Soc. II, 9, 31 (1964).

Shell Effects from A = 40 to 90 (with Bilpuch and Newson), Bull. Am. Phys. Soc. II, 9, 165 (1964).